

**Development of an Artificial Fluorescent Protein Derived from
Photoactive Yellow Protein**

(Photoactive Yellow Proteinを用いた人工蛍光蛋白質の開発)

Doctoral Thesis

September 2014

Dian Novitasari

Graduate School of Materials Science

Nara Institute of Science and Technology

Table of Contents

Chapter 1	General Introduction
Section 1	Photoreceptor Proteins
Section 2	Photoactive Yellow Protein
Section 3	Fluorescent Protein
Section 4	Fluorescence
Section 5	Purpose of this work
Chapter 2	Development of an Artificial Fluorescent Protein Derived from Photoactive Yellow Protein
Section 1	Introduction
Section 2	Materials and Methods
Section 3	Results and Discussion
Chapter 3	Time-Resolved Fluorescence of PYP-coumarin and Two Mutants R52Q-coumarin and E46Q-coumarin
Section 1	Introduction
Section 2	Materials & Methods
Section 3	Results & Discussion
Chapter 4	General Conclusion
Acknowledgments	
List of publications	
References	
Appendix	

Abbreviations

Amino acids

1 letter	3 letter	Name of amino acid
A	Ala	Alanine
C	Cys	Cystein
D	Asp	Aspartic acid
E	Glu	Glutamic acid
F	Phe	Phenylalanine
G	Gly	Glycine
H	His	Histidine
I	Ile	Isoleucine
K	Lys	Lysine
L	Leu	Leucine
M	Met	Methionine
N	Asn	Asparagine
P	Pro	Proline
Q	Gln	Glutamine
R	Arg	Arginine
S	Ser	Serine
T	Thr	Threonine
V	Val	Valine
W	Trp	Tryptophan
Y	Tyr	Tyrosine

PYP	Photoactive Yellow Protein
GFP	Green Fluorescent Protein
pCA	<i>p</i> -Coumaric Acid
TCSPC	Time-Correlated Single Photon Counting
ESPT	Excited-State Proton Transfer
LBHB	Low-Barrier Hydrogen Bond
NMR	Nuclear Magnetic Resonance
SDS-PAGE	Sodium dodecyl sulfate polyacrylamide gel electrophoresis

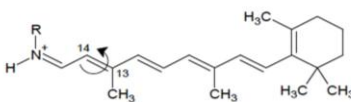
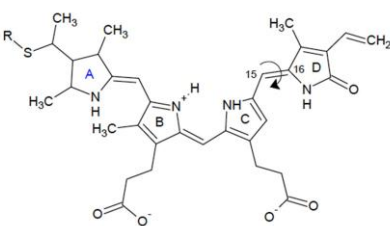
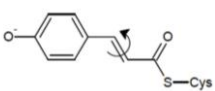
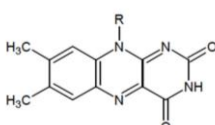
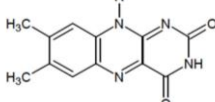
Chapter 1. General Introduction

1.1 Photoreceptor Proteins

Living organisms use light as an energy and information source. Without light, life will not be prosperous on the earth as the present situation. Plants use light in photosynthesis for energy source, and animals use light in vision for information source. The conversion of photon energy into signals is mediated by photo-sensory receptor proteins (or photoreceptors). Chlorophyll proteins are the photoreceptor of photosynthesis and rhodopsin and visual pigments are the photoreceptor of vision. Each photoreceptor protein shows specific color depending on the absorption spectrum. Since protein itself does not significantly absorb visible light, functional activity of a photoreceptor protein depends on a covalently, or non-covalently, associated chromophore to the specific photoreceptor apo-protein. Therefore, wavelength range in which the photoreceptor protein can properly function is determined by this chromophore. The chromophores of above mentioned photoreceptor proteins are chlorophyll and retinal. Other examples of the chromophore are tetrapyrrole other than chlorophyll and flavin. Light absorption by the chromophore triggers the photochemistry which is the basis of structural changes that lead to signal transduction. For example, rhodopsin itself is coupled to G-protein as a transducer protein of receptor-generated signals (1). Beside the photoreceptors specialized in light energy transduction, living organism also uses photosensor protein to monitor the ambient light environment and uses the existing light

conditions optimally for growth and development and/or permits protection against light damage. **Table 1-1** shows an overview of several photosensor families, according to the type of chromophore. In order to extend our knowledge of the photochemistry of photoreceptor proteins, it is important to understand the molecular mechanism after absorbing a photon. The author has used Photoactive Yellow Protein (PYP) as a typical example of blue light sensing proteins and studied the photoreaction of PYP in detail.

Table 1-1. Photosensors families. The arrow indicates in each case the isomerized double bond.

Photosensor family	Chromophore	Chromophore structure	Primary photochemistry
Rhodopsin	Linear polyene (retinal)		<i>Trans-cis</i> isomerization
Phytochromes	Linear tetrapyrrole		<i>Trans-cis</i> isomerization
PYPs	<i>p</i> -coumaric acid		<i>Trans-cis</i> isomerization
LOV	Flavin (FMN)		FMN-cysteinylyl adduct formation
BLUF	Flavin (FAD)		FAD-tyrosine H-bond strengthening
Cryptochromes	Flavin (FAD), pterin (MTHF)		Oxidized FAD

1.2 Photoactive Yellow Protein

Photoactive yellow protein (PYP) was one of the chromophoric proteins which firstly was isolated from the halophilic bacterium *Halorhodospira halophila* strain BN9626 by T. E. Meyer in 1985 (2). This small yellow-colored protein was not identical to any previously reported protein but the absorption spectrum suggested a chromophore similar to flavins. It was shown to be photoactive as the yellow color could be reversibly bleached (2). Although no retinal could be extracted from PYP (3), the photochemical properties of PYP very resembled to the retinal-containing sensory rhodopsins from *Halobacterium halobium* (4). In 1993, the amino acid sequence of PYP from *H. halophila* strain BN9626 was determined and showed that the protein consist of a single peptide chain of 125 amino acid residues with the molecular weight of 14 kDa (5). Like most phototropic organism, *H. halophila* also has a blue light response system, which escapes it away from genetically harmful places, rich in blue light. The action spectrum of this blue light repellent response is close to the absorption spectrum of PYP (6). This observation implies that PYP mediates the photophobic (fear of light) reaction in purple photosynthetic bacterium.

X-ray crystallography has been used to determine the three-dimensional structure of the ground state PYP. It was shown that the protein backbone of PYP is folded in an α/β -fold, with a six-stranded antiparallel β -sheet as the central scaffold, flanked by five elements with α -helical secondary structure (**Figure 1-1**) (7). The loops which connect three

α -helices, fold on top of the β -sheet, and form a major hydrophobic core of the protein (7). The N-terminus of the protein, which includes helices α_1 and α_2 , folds at the back of the central β -sheet to form a second hydrophobic core (7). As a chromophore, PYP binds covalently with *p*-coumaric acid (pCA). Several PYP homologues have been identified in various bacterial species and many more are expected to be revealed since its first discovery more than 25 years ago. However, PYP from *H. halophila* has been well studied in terms of structural and physicochemical properties. Furthermore, it has become the configurational prototype for large and diverse superfamily of sensory proteins generally known as PAS domains (8), which are widely distributed in virtually all forms of life, from humans to bacteria (9).

Generally, when a photosensor protein in the ground state absorbs a photon of the proper wavelength, structural changes occur and lead to a signaling state. From this state, the protein spontaneously returns to its stable ground state. This process is called as photocycle. In the case of PYP, several models for the photocycle intermediates have been introduced, such as in crystals (10), at low-temperature (11), or in a dehydrated state (12). Initially, there are three basic intermediates (13) (see **Figure 1-2**): The first basic step represents the initial photocycle events which the chromophore undergoes photoisomerization. At the end of this first step, the intermediate pR (PYP_L) is formed. The second basic step represents formation of the signaling step, in which the chromophore is protonated, and the structure is changed.

At the end of this step, the intermediate pB (PYP_M) is formed. The third basic step represents the recovery of the ground state (pG), which completes the photocycle (14).

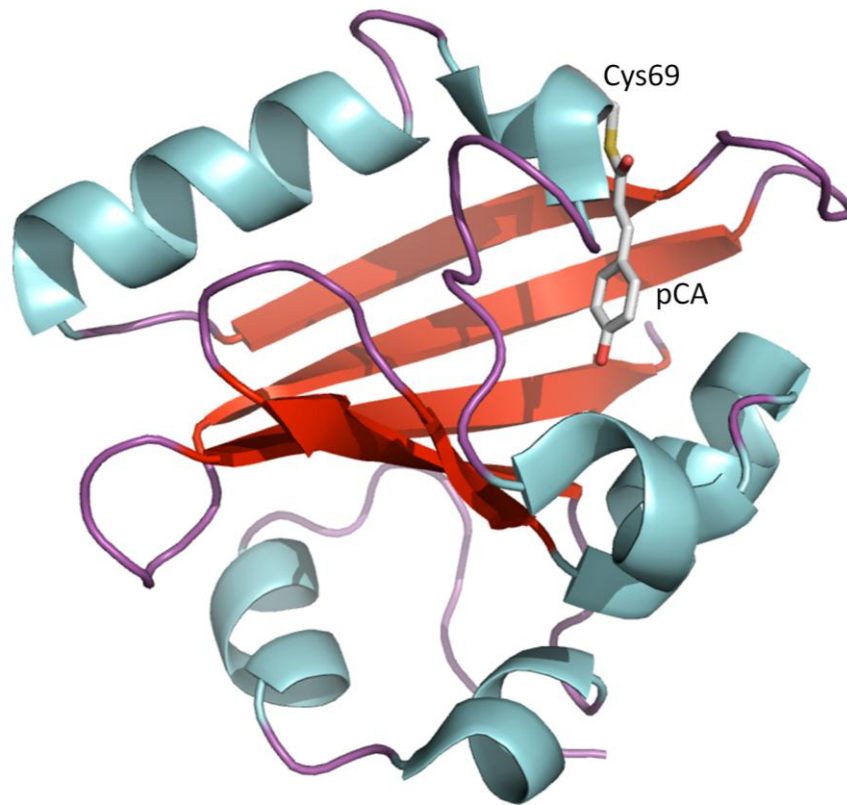


Figure 1-1. Crystal structure of wildtype PYP (PDB entry : 2ZOH). The chromophore pCA is bound to Cys69 via a thioester bond.

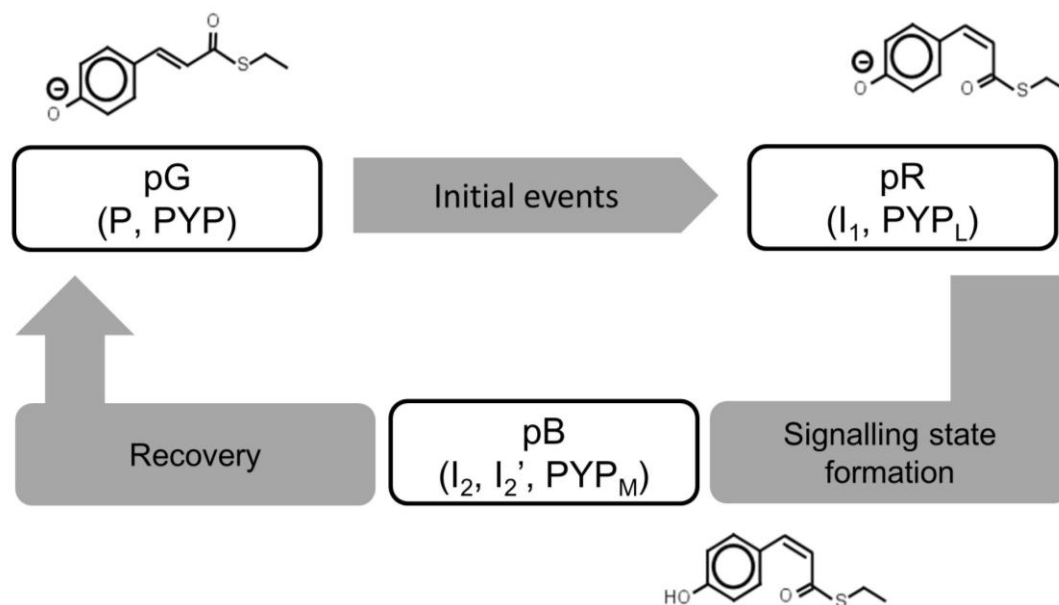


Figure 1-2. Representation of the basic intermediates and events in the photocycle of PYP. (1) the ground or dark state, pG, in which the chromophore is deprotonated and the configuration of the chromophore is *trans*; (2) pR, a red-shifted state (relative to ground state), in which the chromophore is still deprotonated but its isomerization state has changed to *cis*; and (3) pB, a blue-shifted state (relative to ground state), which is presumed to be the signaling state of the photoreceptor. Alternative nomenclatures found in literature are also indicated. Picture was adopted from (14).

The chromophore pCA arranges a hydrogen bond network and interacts with Glu46, Tyr42, and Thr50 (15). The following things of this hydrogen bond network have been revealed by the recent neutron diffraction study of PYP. Based on the position of the deuteron relative to the two pairs of oxygen atoms that form the two hydrogen bonds, it has been concluded that each Tyr42 and Glu46 form a short-ionic (SIHB) and low-barrier hydrogen bonds (LBHB) with the phenolate oxygen of the chromophore (16). Following this publication, solid-state NMR spectroscopy also confirmed the special character of these hydrogen bonds (17). Additionally, previously supposed as a counterion R52, is found to be deprotonated (neutral), and the LBHB has been proposed to stabilize the buried negative charge in PYP (16). As a result, PYP absorbs maximally at 446 nm and the pKa of the chromophore is kept as low as 3.

After absorbing a photon, pCA undergoes *trans-cis* isomerization, which triggers subsequent thermal reactions (9). During the thermal reaction, the hydrogen bond network is modulated, resulting in proton transfers within the network (18). The isomerization is known as one of the fastest chemical reactions, occurs within a few picoseconds, with a reported quantum yield of 0.64 (13), which was later confirmed during the photocycle intermediates study by photobleaching experiments (19, 20). Consequently, it is not surprising that native PYP emits little fluorescence (quantum yield = 3.5×10^{-3} , measured with rhodamine 6G as a standard at room temperature (11); 1.4×10^{-3} (21), and 2×10^{-3} (22)). The emission peak is at

~495 nm (**Figure 1-3**). They also reported that upon measurement at low temperature, the fluorescence quantum yield increased to 0.07 (excitation at 453 nm). Previously, several modifications against the apo-protein and/or the chromophore have been studied with variable success. **Table 1-2** presents a list of all mutants of PYP that have been studied so far, whereas the modification against the chromophore (some reports called as a hybrid) can be seen in **Table 1-3**.

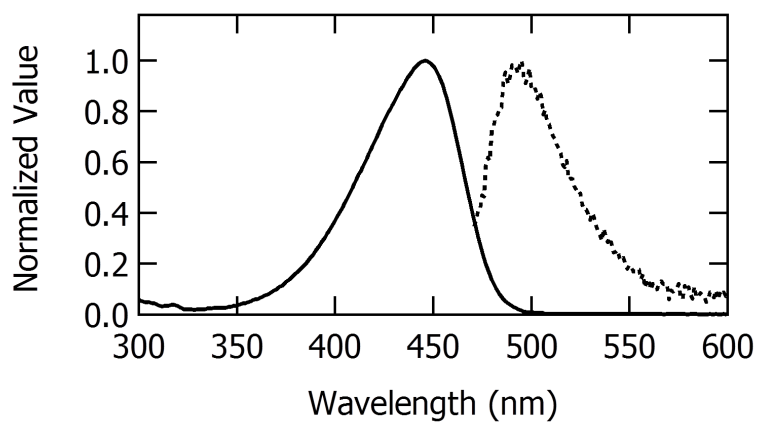


Figure 1-3. Normalized absorption (solid line) and fluorescence emission (dotted line) spectra of native PYP in neutral condition (pH 8.0). The excitation wavelength is set at 446 nm, under room temperature.

Table 1-2. List of all known PYP mutants that have been studied and their absorption maxima.

Mutation	Abs max (nm)	References List
Y42F	391/458	(23-27)
Y42A	375/438	(27)
E46D	444	(28)
E46Q	462	(23, 25, 29-31)
E46A	365/465	(27)
E46X (using 20 amino acid residues)	range from 441 to 478 nm	(32)
G47S	446	(33)
T50A	454	(27)
T50V	457	(27)
E46Q/T50V	472	(27)
E46Q/R52Q	?	(34)
G51S	446	(33)
G47S/S51S	446	(33)
R52A	452	(25)
R52Q	446	(27, 35)
P68A	446	(34, 36)
C69S	-	(23)
M100A	446	(37, 38)
M100E	446	(38)
M100L	446	(38)
M100K	446	(38)
H108F	446	(39)
W119G	445	(34, 36)
Δ 25	444	(40)
Δ 27	444	(40)

Table 1-3. List of chromophores used in PYP that have been studied.

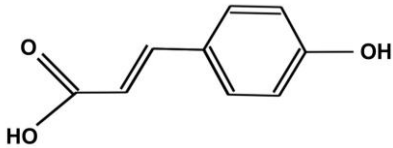
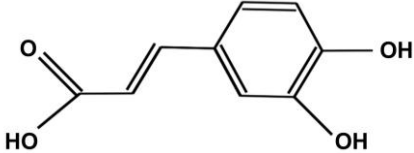
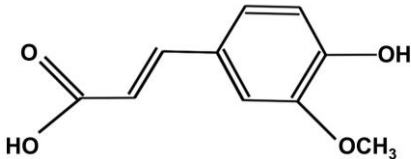
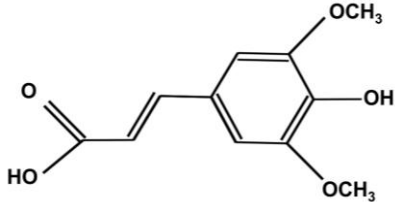
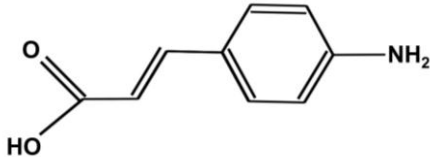
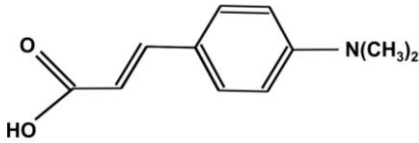
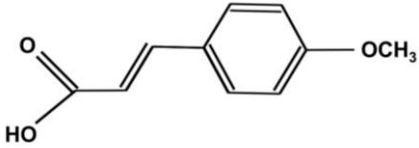
Name of compounds	Structure of free acid
4-hydroxycinnamic acid (22, 41) $\lambda_{max} = 446 \text{ nm}$	
3,4-dihydroxy cinnamic acid (22, 33) $\lambda_{max} = 457 \text{ nm}$	
3-methoxy-4-hydroxy cinnamic acid (22) $\lambda_{max} = 460 \text{ nm}$	
3,5-dimethoxy-4-hydroxy cinnamic acid (22) $\lambda_{max} = 488 \text{ nm}$	
4-amino cinnamic acid (22) $\lambda_{max} = 353 \text{ nm}$	
4-dimethyl amino cinnamic acid (22) $\lambda_{max} = 436 \text{ nm}$	
4-methoxy cinnamic acid (22) $\lambda_{max} = 436 \text{ nm}$	

Table1-3. continued

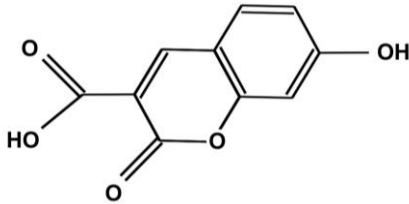
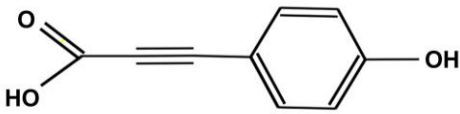
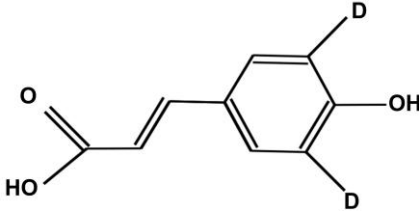
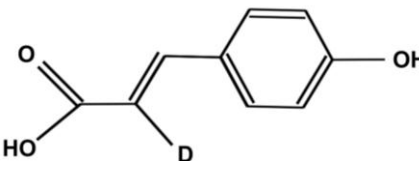
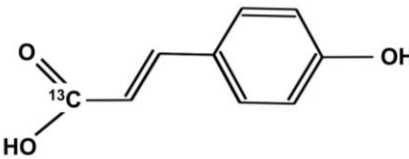
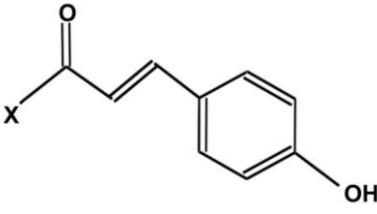
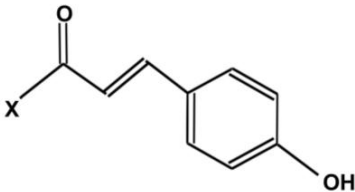
Name of compounds	Structure of free acid
7-hydroxycoumarin-3-carboxylic acid (42, 43) $\lambda_{max} = 443 \text{ nm}$	
4-hydroxyphenylpropionic acid (42) $\lambda_{max} = 404 \text{ nm}$	
<i>p</i> -coumaric-2,6- ² H acid (44)	
<i>p</i> -coumaric-8- ² H acid (44)	
¹³ C-labelled-4-hydroxycinnamic acid (45)	
<i>Trans-p</i> -hydroxycinnamic phenyl thioester (pCTH) (46) X = S-Ph	
<i>Trans-p</i> -hydroxycinnamide (pCMH) (46) X = NH ₂	

Table 1-3. continued

Name of compounds	Structure of free acid
<i>Trans-p</i> -hydroxycinnamic methyl ester (pCEH) (46) X = O-Me	
<i>Trans-p</i> -hydroxycinnamic acid (pCAH ₂) (46) X = OH	
<i>Trans-p</i> -hydroxybenzylidene (pCKH) (46) X = Me	

1.3 Fluorescent Protein

In addition to the photosensor protein families described earlier, there is another type of photo-sensitive protein. This kind of protein can utilize the absorbed photon energy to emit bright fluorescence. This type of protein is called as fluorescent protein. The most famous example of this type is Green Fluorescent Protein (GFP) isolated from coelenterates, such as bioluminescent jellyfish *Aequorea victoria* (47), or the sea pansy *Renilla reniformis* (48). Strictly speaking, the biological function of fluorescent protein is not completely clear. In 1974, Morise and co-workers described that GFP was bound to aequorin, the primary emitter of the bioluminescence (49). GFP absorbed blue light emitted by aequorin and emitted green light by a process called bioluminescence energy transfer (49). The predator might associate such aposematic display like a bioluminescence with a distasteful substance (50). Although some possible roles for fluorescent proteins or GFP-like proteins, such as UV protection (51) or visual mate recognition (52) have been suggested, the clear advantage of the emitted fluorescence for the host or the surrounding ocean is still unknown.

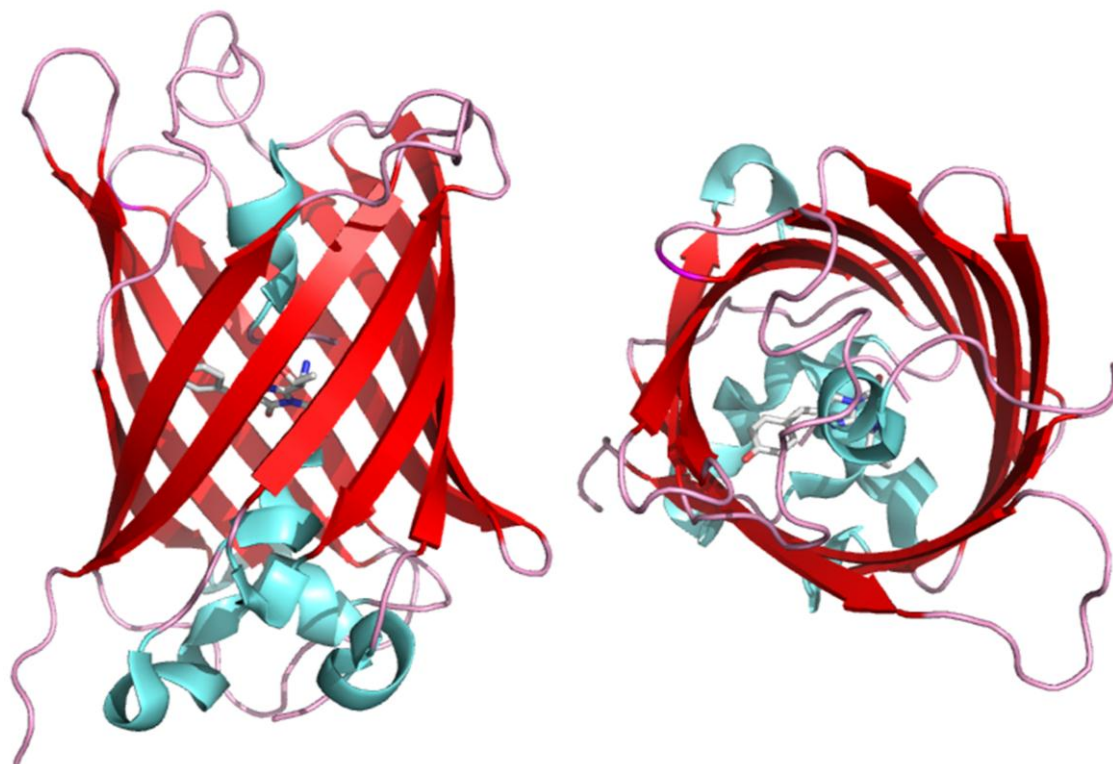


Figure 1-4. Structure of wtGFP from X-ray diffraction analysis (PDB entry : 2B3P). The chromophore of wtGFP buried at the center of the tertiary structure.

The wtGFP consists of a single peptide chain of 238 amino acids and 27 kDa molecular weight that folds in a cylindrical 3D structure, the β -barrel structure (53). Remington group firstly reported the X-ray crystal structure in 1996 revealed that β -barrel of GFP is covered on both ends by short α -helical sections and run through by an α -helix, which comprises the amino acids responsible for the chromophore formation (54, 55). The closed rigid structure of the β -barrel is the key for strong fluorescence of GFP (Figure 1-3) (55). There is an interior cavity filled with water molecules on one side of the central helix, while the other side contains a cluster of hydrophobic side chains (55). Figure 1-4 presents the internal GFP chromophore environment. For the maturation of the chromophore, a number of residues including Thr62 and Gln183 interact and form hydrogen bonds with Arg96 resulting in stabilization of a buried positive charge within the β -barrel, which in turn stabilizes a partial negative charge on the imidazolidone ring (55).

The fluorescing chromophore of GFP, 4-(*p*-hydroxybenzylidene)imidazolidin-5-one (47, 56), originates from the internal cyclization modification of three consecutive amino acids : Ser65-Tyr66-Gly67 (53, 57). This visible fluorescence autogeneration of the GFP has become a mesmerizing success and has been used in various biological fields. Mutation of the sidechains triplet 65-SerTyrGly-67 to other sidechains can be done without loss of function, providing the synthesis of GFP variants with different chromophore structure or its surrounding resulting a wide array of fluorescent tag proteins of

different colors (58) for many applications including painting neurons in a whole colors, known as the brainbow (59, 60).

The main feature of the wtGFP from *Aequorea victoria* is that it shows bimodal absorption spectrum accompanying a large peak at 395 nm ($25,160\text{ cm}^{-1}$, regarded as A-band) and a smaller peak at 475 nm ($20,940\text{ cm}^{-1}$, regarded as B-band), which correspond to the neutral protonated and anionic deprotonated chromophores, respectively (61). It is interesting that GFP emits only green fluorescence regardless of the excitation of the bands. X-ray data of GFP indicate that, in A and B-bands, the chromophore environments is significantly different and it has been proposed that the equilibrium between these states is affected by a hydrogen bond network (**Figure 1-5**) that mediates proton transfer between the chromophore and proximal amino acid residues (62). A proton network that connects the chromophore phenol to Glu222 is active in A state, whereas it is flustered in B state. Upon absorbing photon by B leads to excited state B* that has a single emission at 503 nm. On the other hand, excitation of A, resulting two competing photo-reactions led to large Stokes shift involving direct emission from A* (440-480 nm) and excited state proton transfer (ESPT) from A* to Glu222 through a hydrogen bond network composed of several amino acid residues and a water molecule, leading to 507 nm emission (61).

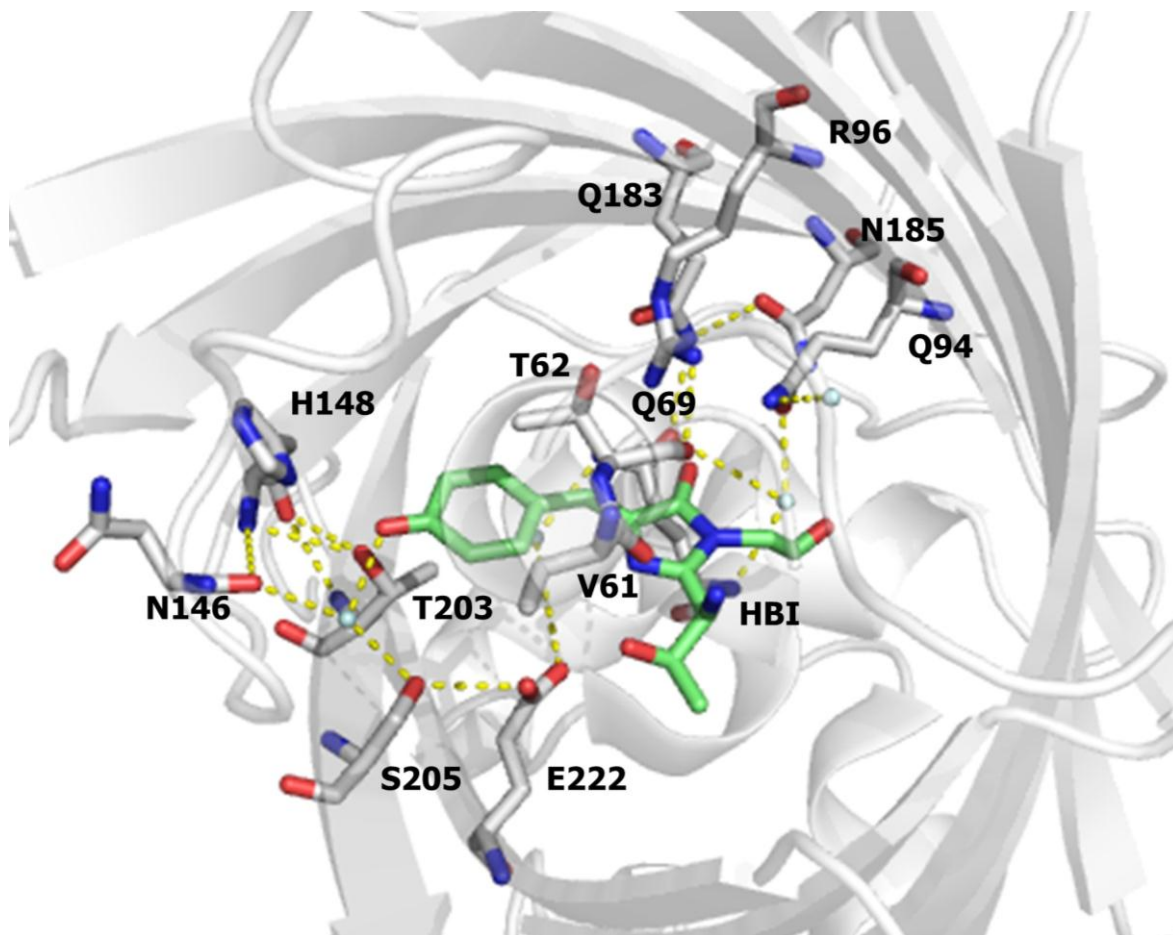


Figure 1-5. Image of hydrogen-bond networks of the internal GFP residues with the chromophore (green) (PDB entry : 2B3P).

1.4 Fluorescence

The main principle of understanding photochemistry is that chemical changes occur when molecular compounds absorb the light. In 1888, the word luminescence was first introduced by Eilhardt Wiedemann, a physicist and science historian, to describe “all those phenomena of light which are not solely conditioned by the rise in temperature”, as opposed to incandescence (63). Luminescence is often considered as cold light whereas incandescence is hot light. Fluorescence is a form of photoluminescence, a spontaneous emission of photons accompanying de-excitation, which is one of the possible physical effects resulting from interaction of light with any substance (63). More specifically, fluorescence is the radiative transition from an excited state to some vibrational level of S_0 , followed by rapid vibrational relaxation to the lowest vibrational level of the ground state. In most cases, the transition is initiated from the lowest vibrational level of S_1 state. Energy distribution of the emitted photon depends on vibrational levels on the S_0 state. Since there is always energy loss of vibrational relaxation at the initial state, the wavelengths of the emitted photons are longer, or at lower energies than those of the absorbed photons. In 1852, G. G. Stokes firstly reported this phenomenon, and thus it referred to the Stokes law (64). However, Stoke’s formulation was only based on relatively simple empirical observations, and the detailed explanation for the practical phenomenon was discovered later.

The spacings between the vibrational levels are (almost) equal in the ground state

and the first singlet excited state. That is why the lowest-energy band of the absorption spectrum (corresponding to $S_0 \rightarrow S_1$ transition) and emission spectrum are mirror images of each other ('mirror image' rule). The difference between the absorption and emission maxima is called the *Stokes shift*, and it is often measured in terms of wavelength (nm) or wave number (in cm^{-1}). For an instance, 7-hydroxycoumarin, a fluorescent compound, has a large Stokes shift of 90 nm. The absorption and emission spectra of 7-hydroxycoumarin, or umbelliferone, are shown with the Stokes shift in **Figure 1-6**, together with the structure of the compound.

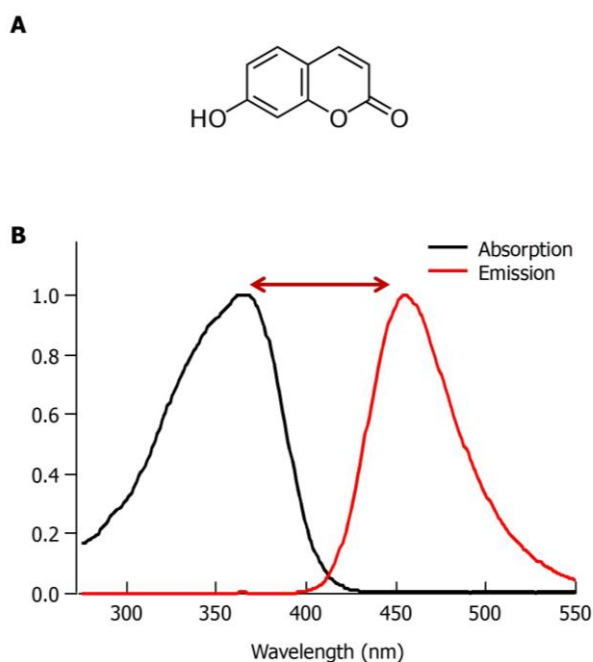


Figure 1-6. (A) Molecular structure, and (B) absorption and emission spectra of 7-hydroxycoumarin. The Stokes shift is depicted by arrow. Excitation wavelength is 365 nm, in 20 mM Tris HCl buffer pH 8.0, RT.

Since the excited state is energetically less favorable than the ground state, the excited electron unavoidably returns back to the ground state. This process is referred as relaxation of the excited state as mentioned earlier. The Perrin-Jablonski diagram (**Figure 1-7**) is usually used for visualizing the possible processes in a simple way, including photon absorption, internal conversion, fluorescence, intersystem crossing, phosphorescence, delayed fluorescence, and triplet-triplet transitions (63). Generally, the transitions can be divided into two categories, namely radiative transitions and non-radiative transitions, represented respectively by the straight arrows and the dotted arrows in the Perrin-Jablonski diagram. In addition to absorption, the radiative processes (involving a photon) include fluorescence and phosphorescence. On the other hand, the non-radiative processes consist of internal conversion (IC), intersystem crossing (ISC), and vibrational relaxation (VR) (63).

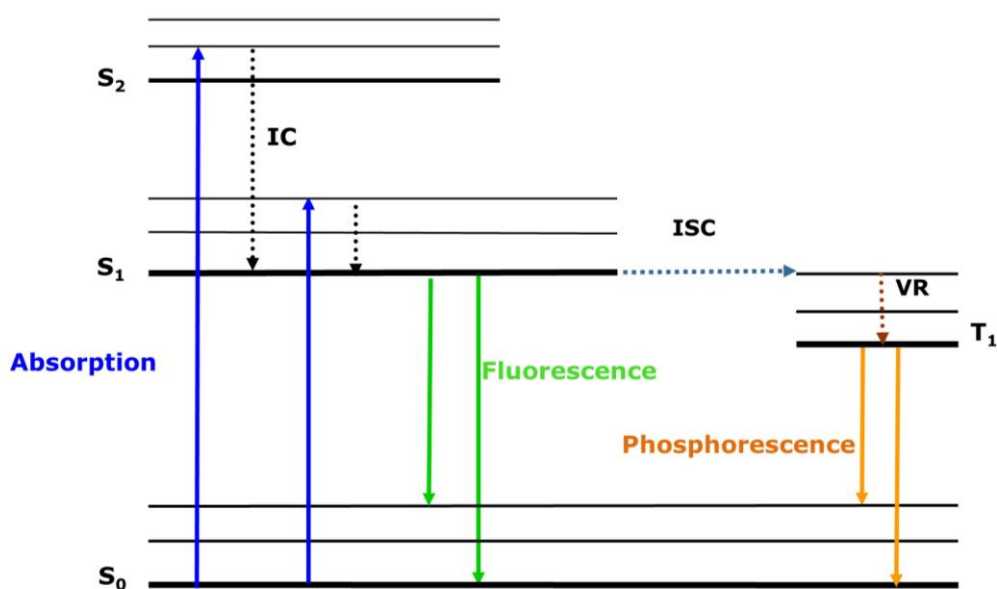


Figure 1-7. Perrin-Jablonski diagram (64).

In this diagram (**Figure 1-7**), fluorescence is the emission of photons accompanying the $S_1 \rightarrow S_0$ relaxation. The emission rates of fluorescence are typically 10^8 s^{-1} , thus a typical fluorescence lifetime is around 10 ns. The lifetime (τ) of a fluorophore is the average time between its excitation and return to the ground state. For simplicity, the author assumes only two electronic state, S_0 and S_1 , and discard vibrational relaxation processes. In the case of a dilute solution of a fluorescent species, the author denotes the concentration of the species in the excited state with $[S_1]$. A very short pulse of light at time 0 brings a certain number of molecules at the S_0 to the S_1 excited state by absorption of photons. These excited molecules then return to S_0 , either radiatively or nonradiatively, or undergo intersystem crossing. Following the classical chemical kinetics, the differential rate law of disappearance of excited molecules is written (63) :

$$-\frac{d[S_1]}{dt} = (k_r^S + k_{nr}^S)[S_1] \quad (1.1)$$

where the corresponding coefficient $k_r^S + k_{nr}^S$ is the sum of the radiative and non-radiative rate constants for the relaxation of the S_1 state. As mentioned above that fluorescence is the radiative relaxation pathway from the S_1 state, thus the rate constant for fluorescence is k_r^S . On the other hand, the non-radiative constant k_{nr}^S , include all non-radiative relaxation pathways from S_1 state, i.e. internal conversion and intersystem crossing from S_1 to a triplet state, T_1 .

This equation can be solved by integration :

$$[S_1] = [S_1]_0 e^{-(k_r^S + k_{nr}^S)t}, \quad (1.2)$$

where $[S_1]$ and $[S_1]_0$ are respectively, the concentration of the excited molecules at time t and at $t = 0$. The lifetime of the excited state S_1 , is given by :

$$\tau_S = (k_r^S + k_{nr}^S)^{-1}. \quad (1.3)$$

Therefore, with this notation, Equation 1.2 can be written as

$$[S_1] = [S_1]_0 e^{-\frac{t}{\tau_S}}. \quad (1.4)$$

Thus, after one lifetime, concentration of the excited molecules has dropped to 1/e or 36.8% of that of the original concentration. The timescale for emitting a photon is as fast as photon absorption ($\approx 10^{-15}$ s) (63). However, the molecule does stay for a certain time (a few tens of picoseconds to a few hundreds of nanoseconds, depending on the type of molecule and the medium) in the excited state before emitting a photon, relaxing back to ground state. The lifetime describes the average time the molecule spends in the excited state before emitting a photon or relaxing by some non-radiative mechanism. Although the relaxation itself is extremely fast, regardless of the mechanism (63).

In addition to the photophysical processes described earlier, in some cases, the excitation also induces chemical reactions. Among various chemical reactions, the most basic reactions are electron transfer and proton transfer (65). For the transfer of a proton or a hydrogen atom happening intra- or intermolecularly, the existence of a proton donor and a

proton acceptor in the molecule has become the most critical requirement. Usually, the proton donor is a hydroxyl group (OH) or an ammonium ($-\text{NH}_3^+$), and the acceptor a carbonyl group (C=O) or a pyridyl nitrogen ($-\text{N}=\text{}$) (65). If the molecules contain both hydrogen-atom donor and acceptor groups in close proximity, hydrogen bond is generally formed in the electronic ground state. In these kinds of molecules, absorbing a photon resulting the redistribution of electronic charge induce an elementary and fast reorganization of the molecular structure, generally referred to as electronically excited-state proton transfer (ESPT).

1.5 Purpose of this work

As described previously, hydrogen-bonding network has an important role in governing the photo-reaction in the excited state. However, little is known about the excited-state reactions in PYP since the native PYP is weakly fluorescent. In this study, to understand the excited-state reactions in the PYP, the author developed the artificial fluorescent PYP and revealed that PYP, under certain conditions, can exhibit large Stokes shift as can be seen in the GFP.

Chapter 2. Development of an Artificial Fluorescent Protein Derived from Photoactive Yellow Protein

2.1 Introduction

Green fluorescent protein (GFP) has been used as an effective tool in various biological fields. It has been reported that the large Stokes shift in wild-type GFP due to an excited-state proton transfer (ESPT) has become a basis for the application of GFP in such techniques as ratiometric GFP biosensors. Previous studies suggest that hydrogen bonding network involving the chromophore of GFP (**Figure 2-1A**) mediates the ESPT event. To examine the relationship between the ESPT and hydrogen bonding network within protein, the author utilized a soluble light absorption protein, PYP, as a model protein. In order to absorb light in visible region, PYP possesses pCA as a chromophore. Since native PYP shows small fluorescence, the first step for the purpose is the development of a strongly fluorescent PYP. pCA undergoes *trans-cis* isomerization upon light absorption, and triggers proton transfer within the hydrogen bonding network (**Figure 2-1 B**). This might be the reason why PYP does not show fluorescence. In this study, the author used a nonisomerizing “locked” chromophore instead of pCA. Coumarin derivatives are good candidate since phenolic oxygen of pCA is important for the structure and photoreaction of PYP. The author chose 7-hydroxycoumarin-3-carboxylic acid (**Figure 2-1 C**) as a locked chromophore.

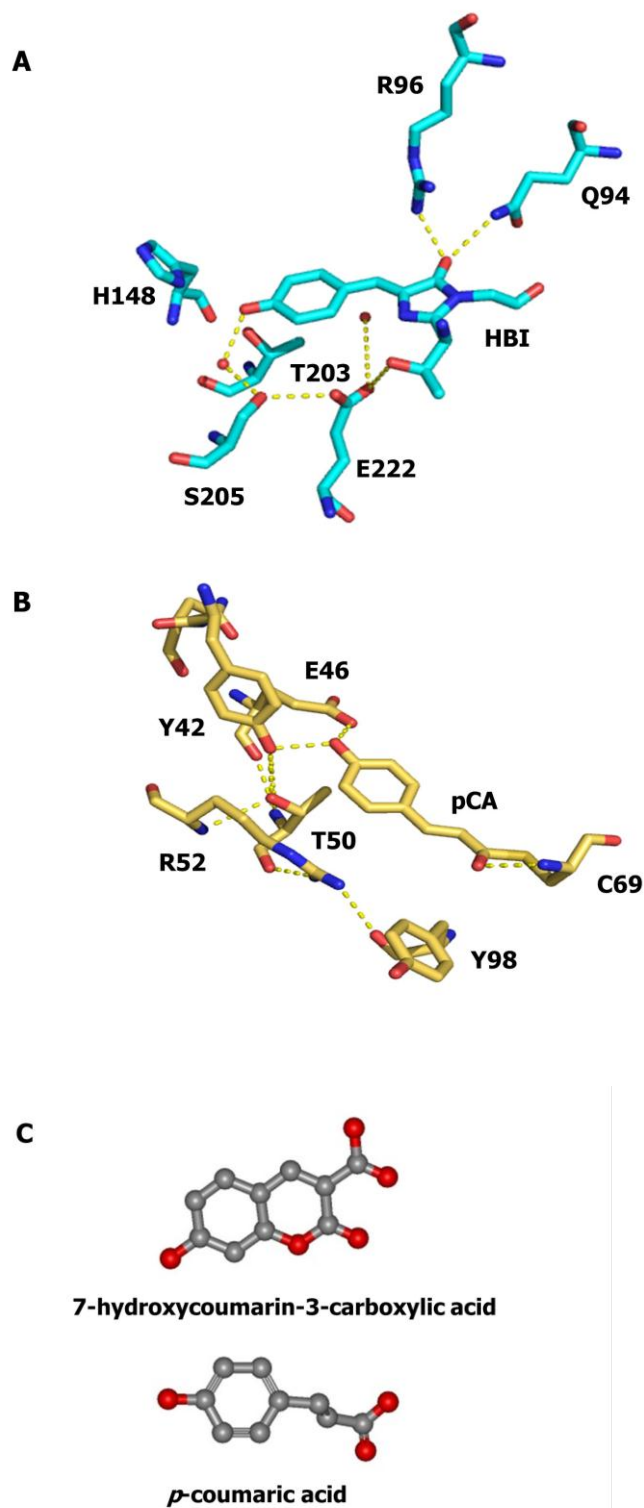


Figure 2-1. Proximal amino acid residues around the chromophore environment that involves in hydrogen-bond network formation in (A) GFP and (B) PYP. (C) Chemical structure of 7-hydroxycoumarin-3-carboxylic acid and *p*-hydroxycinnamic acid (pCA).

2.2 Materials & Methods

Expression and purification of the proteins

PYP was overexpressed using the pET system in *Escherichia coli* BL21(DE3) (Novagen), and reconstituted with anhydrous 7-hydroxycoumarin-3-carboxylic acid in 4 M urea buffer, according to the standard protocol used for obtaining the native PYP (23). *E. coli* cells BL21(DE3) containing pET-PYP were cultured at 37°C in 2xYT medium containing 50 μ g/ml ampicillin. Expression of PYP was induced by the addition of isopropyl-thio- β -galactoside (IPTG). After about 3~4 hours, cells were harvested by centrifugation at 4000 RPM for 20 minutes. Harvested cells were suspended in the extraction buffer (8 M Urea, 25 mM Tris HCl, pH 8.0) and centrifuged for 30 min, at 4°C. The supernatant obtained was then diluted by the addition of equivalent volume of dilution buffer (20 mM Tris HCl, pH 8.0), followed by addition of 7-hydroxycoumarin-3-carboxylic acid anhydride. The reconstitution was carried out gently, and stirred on ice for at least 30 min. The coumarin analog (7-hydroxycoumarin-3-carboxylic acid) was directly purchased from Lambda. After addition of 7-hydroxycoumarin-3-carboxylic acid anhydride, the reaction mixture turned yellow. The PYP reconstituted with 7-hydroxycoumarin was purified by ion-exchange chromatography using DEAE Sepharose CL6B column chromatography (60 mm diameter, 21 cm length, and 42 ml volume) (Amersham Biosciences), loading and washing with 20 mM Tris HCl pH 8.0 buffer; elution with 20 mM phosphate buffer with 500 mM NaCl, pH 8.0; temperature 4°C.

The optical purity index of obtained protein ($\text{Absorbance}_{280}/\text{Absorbance}_{\lambda_{\text{max}}}$) is approximately 0.5. Using this purity index value, preliminary small crystals of PYP-coumarin can be obtained (**Figure 4-1**). The purified sample was dialyzed against a buffer containing 20 mM Tris-HCl, pH 8.0. The binding ability of 7-hydroxycoumarin-3-carboxylic acid to apo-PYP was assayed by SDS-PAGE. Native PYP has an apparent molecular weight of 18,800 on SDS-PAGE, while its mass is 14,000 Da (66).

Absorption and fluorescence spectroscopies

UV-Vis absorption spectra and fluorescence spectra were measured immediately after adjusting the pH of the sample. A small volume of HCl solution (0.1 M–1 M) was added to the sample cuvette. The resultant pH values were measured by putting a small portion of the sample on the electrode of a compact pH meter (Laqua Twin B-712, Horiba, Ltd.), as described in a previous report (27). Absorption spectra were measured with a UV2450 spectrometer (Shimadzu). The fluorescence spectra were measured using an RF5300PC spectrofluorometer (Shimadzu).

2.3 Results & Discussion

In this study, reconstitution of the PYP-coumarin was carried out according to published report (23). The sample was purified firstly by manual open column chromatography and followed by HPLC system using DEAE column. **Figure 2-2** shows the

final HPLC profile of purified PYP-coumarin. The binding ability of wild-type apo-PYP to the 7-hydroxycoumarin-3-carboxylic acid was confirmed by **Figure 2-2**, because the signals from protein (280 nm) and coumarin (444 nm) appear at the same fraction. **Figure 2-3** shows the result of SDS-PAGE analysis for the native PYP (**Figure 2-3A**) and PYP-coumarin (**Figure 2.3B**). Both of these figures show similar band at ~18,800. Based on these figures, I concluded that the reconstitution of PYP-coumarin succeeded.

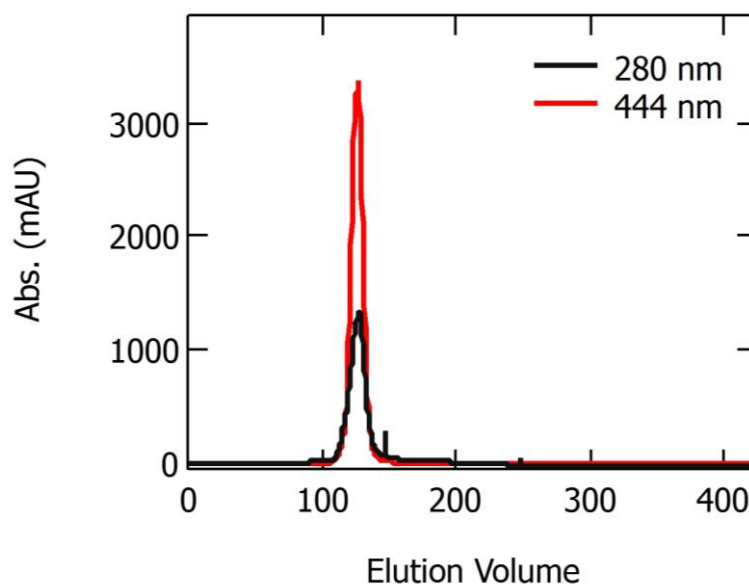


Figure 2-2. Elution curves of wtPYP-coumarin. The elution curve was obtained by ion-exchange chromatography (DEAE Sephadex CL6B column chromatography, 60 mm diameter, 21 cm length, 42 ml volume) using HPLC system. Conditions : flow rate 1 mL/min; monitoring wavelength 280 nm and 444 nm; loading and washing with 20 mM Tris HCl pH 8.0 buffer; elution with 20 mM phosphate buffer with 500 mM NaCl, pH 8.0; temperature 4°C.

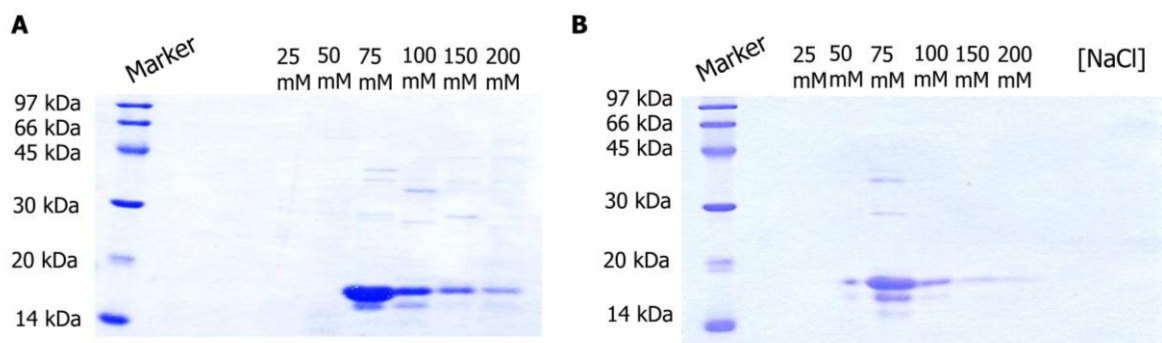


Figure 2-3. SDS-PAGE analysis of native PYP (**A**) and PYP-coumarin (**B**). The gel was stained with Coomassie Brilliant Blue (CBB). The reconstitution of PYP-coumarin succeeded.

PYP-coumarin absorbs maximally at 444 nm, which is close to that of the native PYP (446 nm) (**Figure 2-4**). The spectral bandwidth of PYP-coumarin is narrower than that of PYP, which is partly due to the planarity of the π -conjugate bond in 7-hydroxycoumarin-3-carboxylic acid. Upon lowering the pH, the blue-shifted species with the λ_{max} of 378 nm gradually accumulated (**Figure 2-5A**). The pKa value for the protonation of the phenolic oxygen in this reconstituted PYP-coumarin was determined by fitting the pH dependent absorption to the Henderson-Hasselbalch equation (67). The appearance of a clear isosbestic point at 402 nm (**Figure 2-5B**) indicates that the reaction is a 2-state transition, where the pKa value was 2.86 ($n=1.50$). The native PYP also exhibits similar spectral changes upon decreasing the pH and pKa value was also ~ 3.0 (27), in another study the pKa value was 2.7 ($n=1.9$) (43). The spectral change reflects an alteration of the protonation state of pCA. The chromophore of the native PYP forms a low-barrier hydrogen bond and partly deprotonated (16) at neutral pH and protonated at acidic pH. Based on this knowledge, the author considers that the chromophore of PYP-coumarin is deprotonated at neutral pH and protonated upon decreasing the pH.

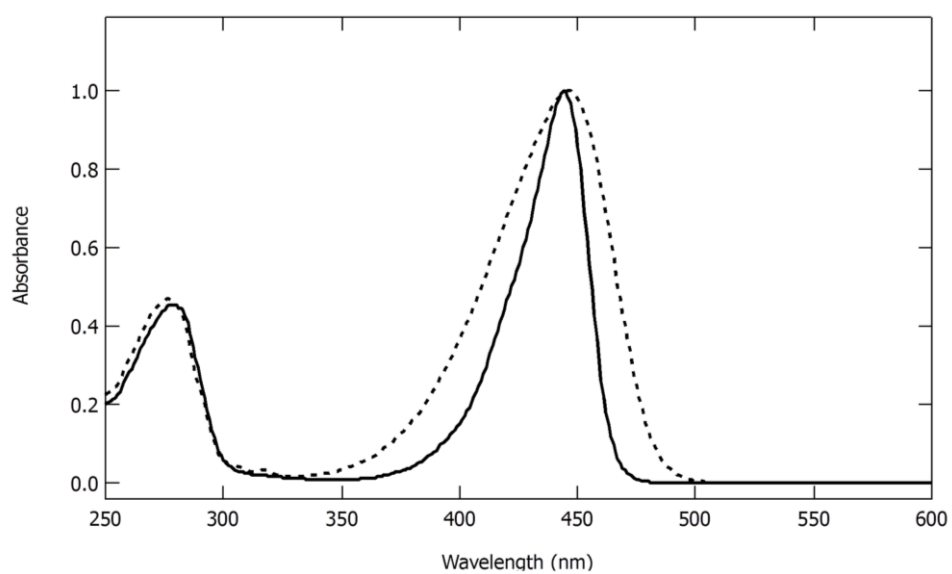


Figure 2-4 Normalized UV-Vis absorption spectra of PYP-coumarin (solid line) and the intact PYP (dashed line) measured at pH 8. The buffer condition is 20 mM Tris-HCl.

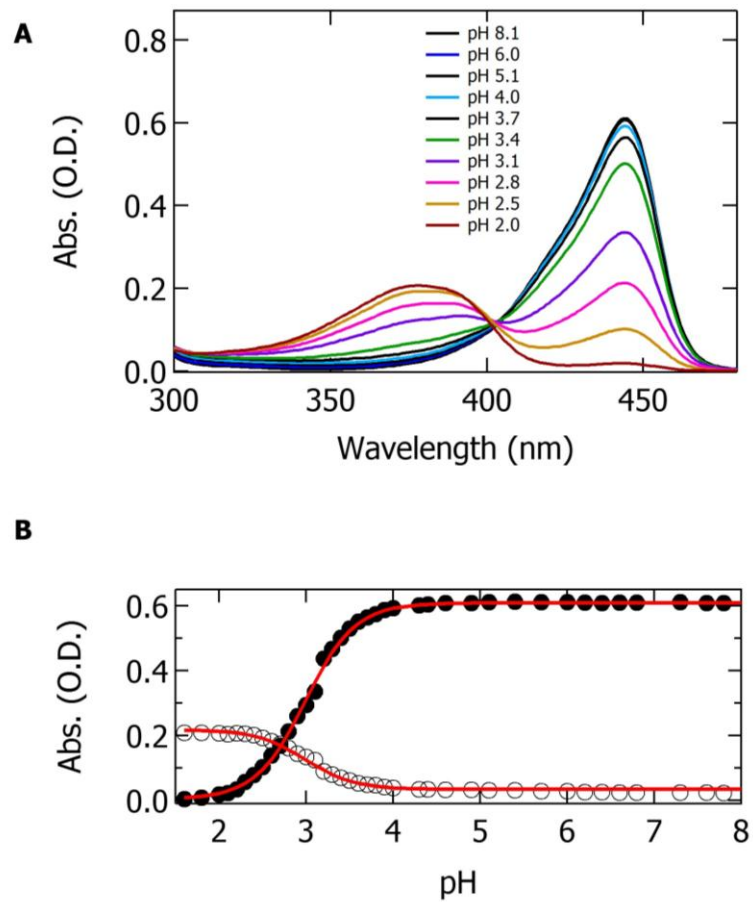


Figure 2-5 (A) UV-Visible absorption spectra of PYP-coumarin measured at pH 2.0, 2.5, 2.8, 3.1, 3.4, 4.0, 6.0 and 8.1. (B) Titration curves monitored at 444 nm (filled circle) and 378 nm (open circle). The buffer condition is 20 mM Tris HCl, RT.

Although the pK_a value of free 7-hydroxycoumarin is about 8, the protein environment of PYP-coumarin stabilized the anionic form of 7-hydroxycoumarin to lower the pK_a value by 5 pH units. The λ_{max} value of PYP-coumarin is red-shifted by about 100 nm from the value of the deprotonated form of free 7-hydroxycoumarin (365 nm). These results indicate that 7-hydroxycoumarin is actually embedded in the protein interior, similarly to the native PYP, and forms hydrogen bonds with the proximal amino acid residues.

The fluorescence intensity of the PYP-coumarin was about 25 times larger than that of the native PYP under the same condition (**Figure 2-6**). This result confirms that the loss of isomerization ability of the attached chromophore increases the fluorescence efficiency. The photograph of PYP-coumarin is also shown in **Figure 2.7**.

Figure 2-8A shows the emission and excitation spectra of PYP-coumarin at pH 2.2 and 4.2, where the protonated and the deprotonated chromophores are mainly accumulated, respectively. In this figure, in order to obtain the emission spectra, the wavelength of the excitation light was set at 444 nm. By using this excitation wavelength, only the deprotonated PYP-coumarin can primarily absorb light. Only weak emission at pH 2.2 was observed, due to a small fraction of deprotonated form of PYP-coumarin at pH 2.2. The emission and excitation spectra at pH 4.2 looks like mirror symmetry (line 1 and line 2 of **Figure 2-8A**), which is the ordinary relationship between emission and excitation spectra. On the other hand, the spectra at pH 2.2 exhibited an asymmetric relationship, where the spectral shape of the

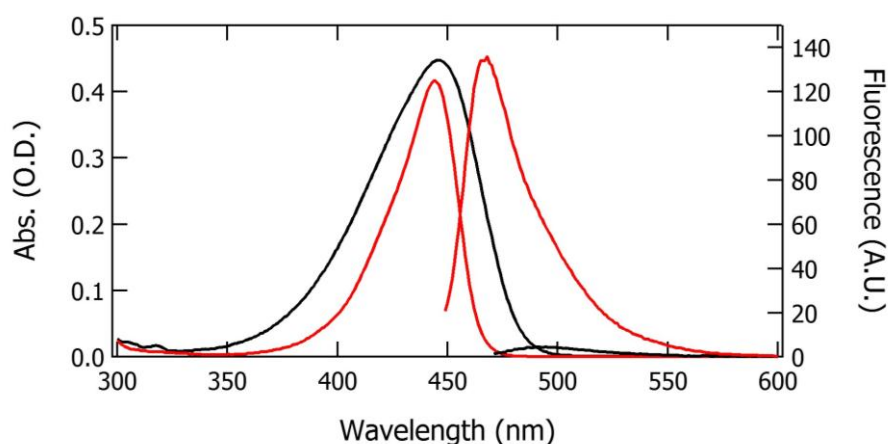
emission was almost identical to that at pH 4.2, except for the intensity, but the excitation showed large intensity at around 380 nm (line 3 and line 4 of **Figure 2-8A**). The λ_{max} was almost identical to that of the UV-Vis absorption spectrum of the protonated PYP-coumarin, indicating that the protonated PYP-coumarin emits strong fluorescence at 468 nm, even though the λ_{max} of the protonated form (378 nm) was substantially blue-shifted by ~ 70 nm, as compared with that of the deprotonated form (444 nm).

The emission spectrum at pH 2.2 excited at 350 nm is shown in **Figure 2-8B**, line 1. The protonated form could mainly absorb blue light. The emission spectrum at pH 2.2 showed a characteristic bilobed shape, accompanying a major peak at 463 nm and a broad peak at around 430 nm. The major peak was found to give rise to the large intensity in the excitation spectrum monitored at 468 nm under the acidic condition (**Figure 2-8A**, line 4). The λ_{max} of the major peak was almost identical to the λ_{max} of the fluorescence peak of the deprotonated PYP-coumarin (468 nm). Therefore, the major peaks arise from the same excited state of the deprotonated PYP-coumarin at pH 4.2; namely, ESPT occurs in the protonated PYP-coumarin. Using the fluorescence spectra at pH 2.2 and 4.2, the remaining fluorescence spectrum in the bilobed shape was reconstituted (line 3 in **Figure 2-8B**). The calculated spectrum shape was likely to be a mirror symmetrical shape against the UV-Vis spectrum of the protonated chromophore, indicating that the shoulder at around 430 nm arises from the excited state to ground state transition of the protonated chromophore at the excited

state. These results indicate that the protonated PYP-coumarin shows dual emission arising from the protonated and deprotonated forms at the excited state, the latter of which is realized by the ESPT. The ESPT efficiency can be calculated roughly from the steady state measurement. The ESPT efficiency of protonated PYP-coumarin is not 100%, since the emission showed dual maxima with a peak at 465 nm, and a broad peak at ~430 nm. Comparing these two emission intensity values, ESPT efficiency of PYP-coumarin is approximately 60%, measured at pH 2.1, in 20 mM Tris HCl, RT.

Figure 2-9 presents the proton transfer mechanisms of protonated PYP-coumarin in a simplified way. In this figure, S_0 and S_1 refer to the ground state and first singlet excited state of the protonated form of PYP-coumarin, and S'_0 and S'_1 to the ground state and the first excited state of the deprotonated form, respectively. The solid lines with arrows depict the protonated form absorption and deprotonated form fluorescence. To some extent, the excited state of the protonated form, also called *the locally excited state*, relaxes directly back to its ground state. There is a weak fluorescence emission as well, which might be from the protonated form emission, shown by the dashed arrow in **Figure 2.9**. For the protonated form of PYP-coumarin, the absorption maximum (in water containing Tris HCl pH 2.1) is located at 378 nm and the emission is maximized at 465 nm. Therefore, the Stokes shift is large : 87 nm. Generally, the proton transfer is so rapid that in steady-state measurement the normal tautomer fluorescence is not observed. However, protonated PYP-coumarin at excited state

exhibits dual emission meaning that not only the reaction product band can be observed. At this stage, the proton acceptor after ESPT is still unknown. The possible candidates might be E46, R52 or water molecule around the chromophore (see **Figure 2-1B** for detailed structure).



System	Absorbance	Emission Intensity
Native PYP	0.448	4.6
PYP-coumarin	0.417	136

Figure 2-6. Emission spectra of PYP-coumarin (red line) and native PYP (black line). The absorption spectra are also described here. Detailed values for each spectrum are shown in the table. Emission spectra excited at 444 and 446 nm for PYP-coumarin and native PYP, respectively. The buffer condition is 20 mM Tris HCl pH 8.0, RT.

Native PYP PYP-coumarin

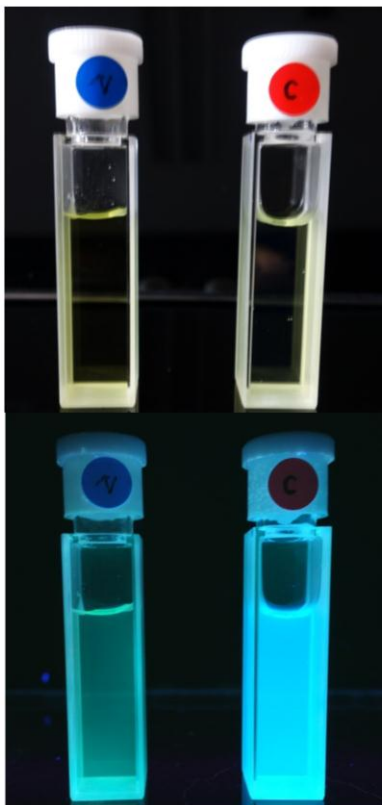


Figure 2-7. Photographs of native PYP and PYP-coumarin under ambient (top) and UV light (bottom).

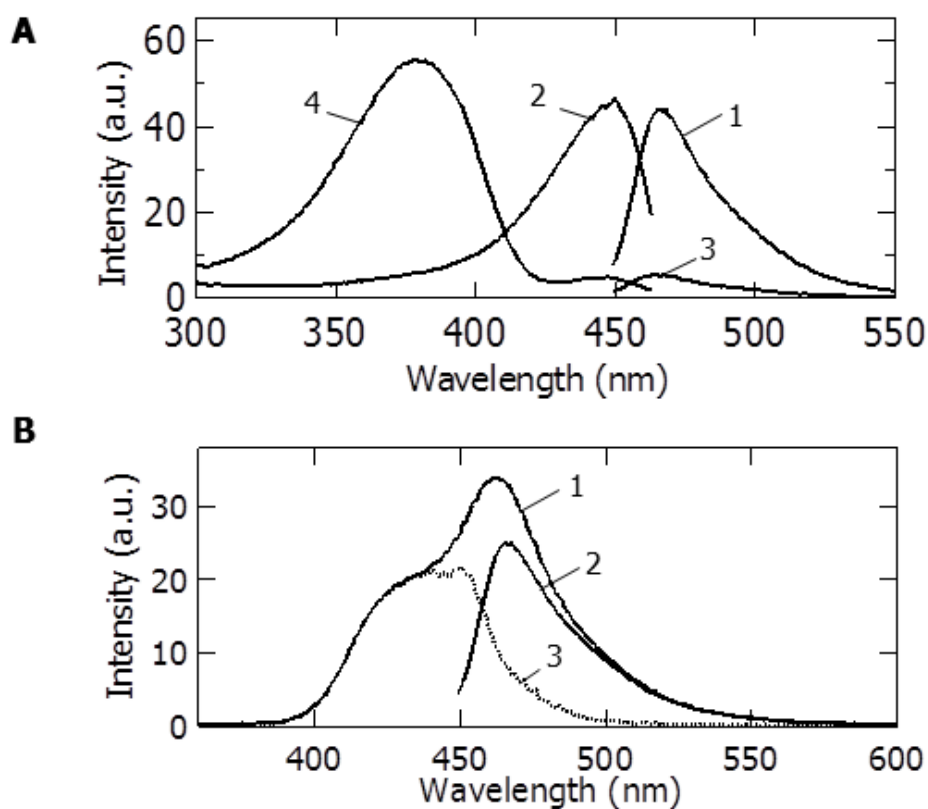


Figure 2-8 (A) Line 1 and 3 are fluorescence emission (excitation wavelength is 444 nm) spectra of PYP-coumarin at pH 4.2 and pH 2.2. Line 2 and 4 are excitation spectra of PYP-coumarin (emission wavelength at 468 nm) measured at pH 4.2 and pH 2.2. (B) Emission spectra of PYP-coumarin (excitation wavelength is 350 nm) at pH 2.2, line 1. Line 2 is the emission spectrum of PYP-coumarin (excitation wavelength is 444 nm) measured at pH 4.2. The calculated emission spectrum, line 3, obtained by subtracting the scaled emission spectrum of the deprotonated excited state (line 2 from line 1). The buffer condition is 20 mM Tris HCl, RT.

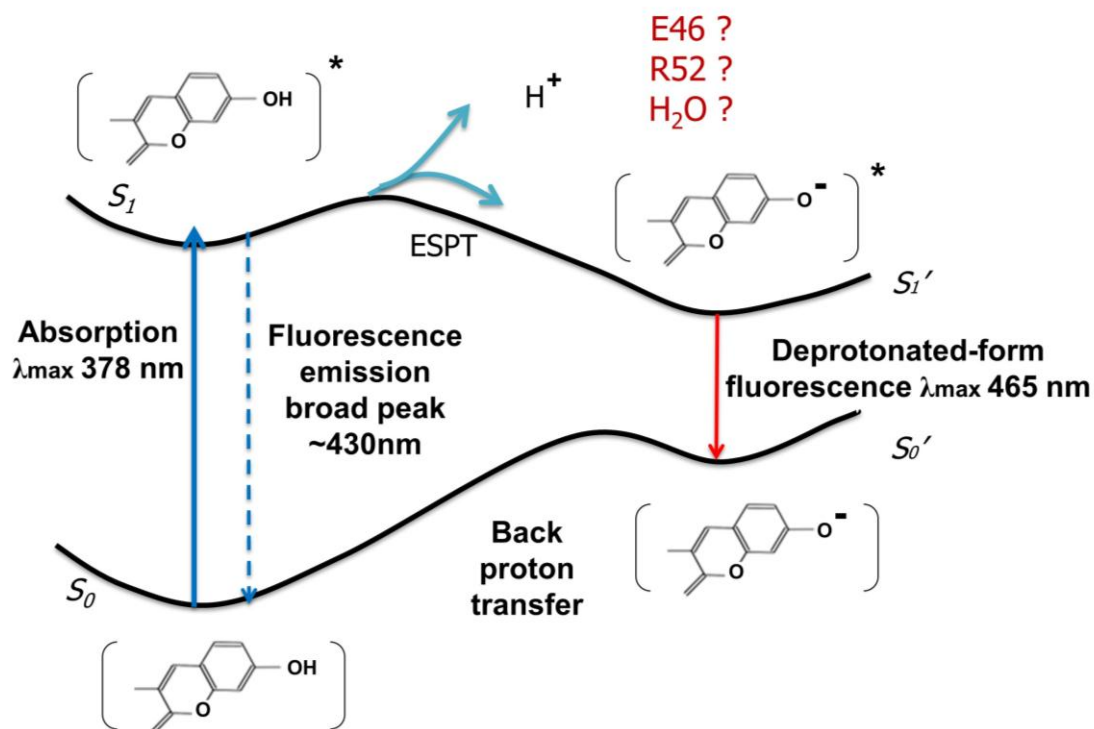


Figure 2-9. A simplified scheme of the energy profiles associated with excited-state proton transfer in protonated PYP-coumarin in acidic condition. The possible proton acceptor candidates are also indicated in this figure.

Chapter 3. Time-Resolved Fluorescence of PYP-coumarin and Two Mutants

R52Q-coumarin and E46Q-coumarin

3.1 Introduction

Hydrogen bond interaction and associated intramolecular process like ESPT following the photoexcitation in PYP-coumarin might reflect the chromophore environment in the protein. In order to get a better image of the fluorescence spectral evolution of the reconstituted PYP-coumarin, the static measurement needs to be supported by the time-resolved fluorescence measurements. Among various methods available in this field, time-correlated single photon counting (TCSPC) with a streak camera system is quite attractive. By using this system, the complete time and wavelength spectral profiles can be obtained in one single measurement. The first part of this chapter will exhibit the time-resolved fluorescence of wtPYP-coumarin at pH 2.1 in line with the previous static measurement of the previous chapter. Since the point mutation is a powerful tool to examine the roles of each amino acid residue, the effect of hydrogen bonding network to the fluorescence efficiency was also investigated by comparing the fluorescence properties of the wtPYP-coumarin and two mutants : R52Q-coumarin and E46Q-coumarin. These two residues are located near the chromophore pCA (**Figure 2-1**) and involved in the hydrogen bond network. These residues may serve as either a proton donor or an acceptor. Therefore, these two mutants are expected to influence the hydrogen bonding network around the

chromophore in PYP-coumarin. They are also expected to affect the ESPT efficiency.

3.2 Materials & Methods

Expression and purification of the proteins

Wild-type PYP and two mutants R52Q and E46Q were overexpressed using the pET system in *Escherichia coli* BL21(DE3) (Novagen), and reconstituted with anhydrous 7-hydroxycoumarin-3-carboxylic acid in 4M urea buffer, according to the standard protocol used for obtaining the native PYP (23). All samples were diluted with Tris HCl buffer (at neutral and acidic pH).

Time-resolved emission spectroscopy

In addition to static measurements, time-resolved measurements were performed to study the ESPT reaction. Since the fluorescence intensity is proportional to the population of the excited state, measuring the time profile of the emission provides a means to monitor the reaction dynamics of photo-chemical reactions (68). One of the most widely used methods for time-resolved emission measurements in the nanosecond and sub-nanosecond time domains is the single photon timing technique or also known as time-correlated single photon counting (TCSPC) (68).

The TCSPC method is based on the fact that the probability of a photon reaching a detector after an excitation pulse after some time t is proportional to the fluorescence intensity at that time (68). Therefore, using TCSPC method, we cannot obtain absolute values

of the fluorescence intensity at different times, but only a time profile for the decay of the fluorescence emission. **Figure 3-1** represents a schematic view of a TCSPC system (68). The excitation light is split by the semi-transparent mirror M_1 . Part of the beam is directed to a photodiode (PD) and converted to an electric pulse. A constant factor discriminator (CFD) which uses a constant fraction of the input pulse, ensures that timing of the signal at the CFD output does not depend on the amplitude of the input pulse (68). The signal is then directed to a time-to-amplitude converter (TAC), which generates a voltage increasing linearly with time (68). The rest of the pulse excites the sample. The emitted light is directed to a monochromator, and to the photomultiplier tube (PM). The electric signal from the PM is directed through a second CFD to the TAC, and stops the voltage increase (68). The generated voltage is then analyzed by a multichannel analyzer (MCA) (68).

The fluorescence lifetimes of the proteins were measured using an assembly of a Hamamatsu-C4334 and C5094 photon-counting streak-scope. The excitation source used for lifetime measurements provided 365 and 444 nm pulses (150 fs) generated from the SHG crystal of a Coherent OPA optical parametric amplifier. The OPA was pumped by a Coherent regenerative amplifier which was seeded by a mode-locked Coherent Mira Ti:Sapphire laser. All measurements were done under room temperature. Lifetime fluorescence decay data were analyzed using global analysis method using the Igor Pro 6.34A software (WaveMetrics, Oregon, USA). The TCSPC measurements were carried out in the same fluorescence cuvettes

as the steady-state emission measurements.

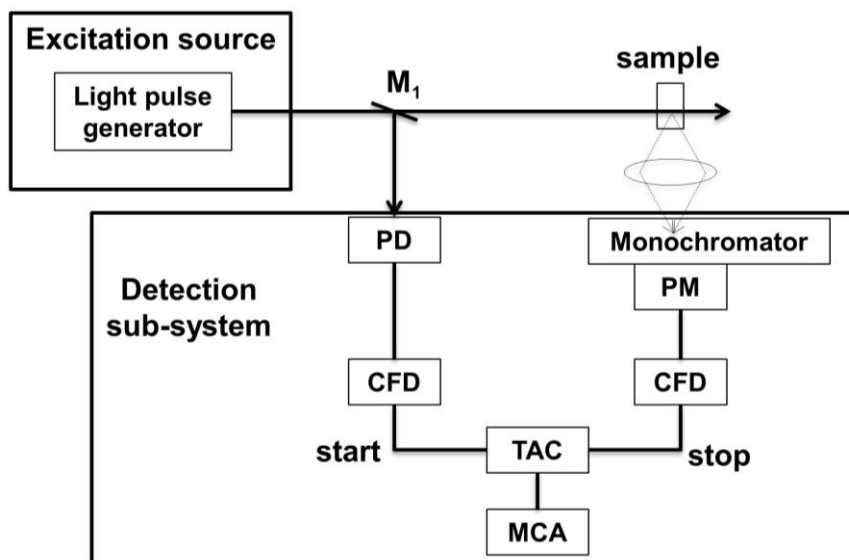


Figure 3-1. Scheme of a time-correlated single photon counting (TCSPC) system. M_1 is a semi-transparent mirror, PD is a photodetector, PM is a photomultiplier tube, CFD a constant fraction discriminator, TAC a time-to-amplitude converter, and MCA a multichannel analyzer (68).

Far-UV CD Spectra

Far-UV circular dichroism (CD) spectra were measured with a JASCO model J-820 spectropolarimeter. Sample used in the CD were exactly the same sample of the time-resolved emission measurements. The sample was put into a quartz cell with a light path length of 1 mm. The temperature of the sample was kept at 20°C using a peltier device.

3.3 Results and Discussion

Confirmation of the existence of ESPT

Figure 3-2A represents the fluorescence emission decay curve obtained from TCSPC measurement for wtPYP-coumarin at pH 2.1. Reconstruction of the fluorescence spectrum has been done by analyzing the decay with a double-exponential function at each wavelength and then reconstructing the spectral components (**Figure 3-5B**). **Figure 3-5B** shows that there are two independent emission spectra with only single peak of each spectrum. The fast component (red dotted lines) has a single emission at ~440 nm, while the slow component (blue dotted lines) has a peak at ~470 nm. The static measurement of neutral form at pH 8.0 emits maximally at 467 nm, suggesting that slow component obtained from acidic condition is corresponding to the neutral form emission spectra from the steady-state measurement. In this figure, the latter emission spectra are also superimposed (blue solid line).

Comparable spectra shape between this slow component and the emission of

deprotonated form, leads to the conclusion that it is resulted from the same excited-state, i.e. deprotonated excited state. On the other hand, since the decay time of the fast component is very close to the instrumental response, the attribution of fast component to the protonated form emission is suggestive, not conclusive. Similar interpretation in attribution of the spectral components obtained from the time-resolved fluorescence measurement persists to the result of mutants R52Q-coumarin and E46Q-coumarin in the following section.

As described above, spectral components of wtPYP-coumarin measured at pH 2.1 can be clearly divided into two independent components, the lifetime constants obtained here were ascribed as the fluorescence lifetime of protonated and deprotonated form in the excited state. The latter emission peak is correlated well with the peak of the bilobed shape spectrum at acidic pH obtained from the static measurement (see Chapter 2). Based on these facts, the author concludes that there are two phases of the fluorescence emission. These two can be attributed to the lifetime from the two different excited-state, one is protonated state, the other one is deprotonated state in the excited state, since the ground state of the chromophore is protonated state, the deprotonated excited state is realized by the ESPT. However, there is no direct evidence to determine the rate of ESPT in this time region. The shortest fluorescence lifetime of 383 ps, which correlated to the emission peak at ~440 nm, cannot be associated directly to the relaxation of the enol excited state. Therefore, the rate of the ESPT reaction cannot be determined using the current time resolution. If the lifetime measurement with

much faster time region than the current resolution can be conducted, probably the ESPT rate can be determined. Usually, ESPT is a very rapid that only the reaction product band is seen in the fluorescence spectra. However, such cases are not interesting for designing the fluorescence reporters. Fluorescence reporter with dual emission is more attractive, and this phenomenon is observed in two cases (69). First, when the initially excited state becomes the intramolecular charge transfer (ICT) state stabilized to be of similar energy as the ESPT product state, then the ESPT reaction becomes reversible and an equilibrium between two forms can be established on a timescale faster than the emission (69). For an instance, 3-hydroxyflavone derivatives show this kind of behavior (70). Second, the product of the ESPT reaction exhibits slow kinetics on the timescale of emission, which may be due to intramolecular hydrogen bonding perturbations of chromophore (69).

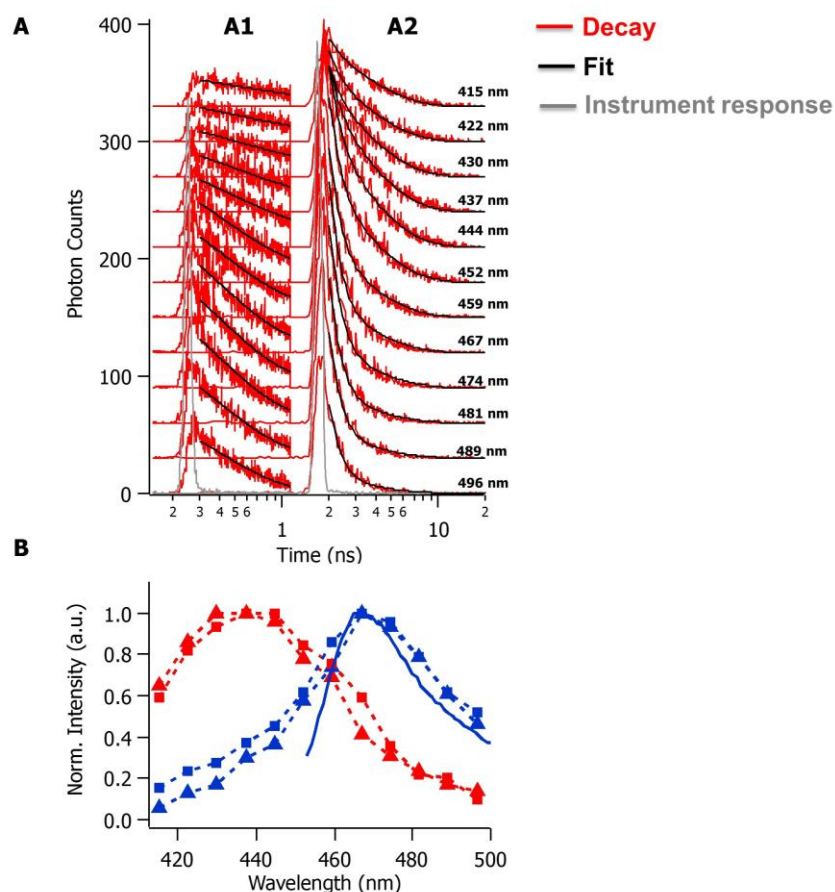


Figure 3-2 A. Fluorescence emission decay curves (red lines) of wtPYP-coumarin pH 2.1 fitted using global analysis with double exponential functions. Excitation wavelength is 365 nm, with time window 1 ns (**A1** panel) and 20 ns (**A2** panel). The black lines indicate the fitted curves, and the grey line is the instrumental resolution. **B.** Reconstructed spectral component obtained by analyzing the decay with double exponential functions using global analysis, normalized to the same intensity value (see **Appendix 4** for details). Fast and slow fluorescence components are shown by red and blue dotted lines, respectively, for both 1 ns (triangle) and 20 ns (square) time windows. The emission spectra of neutral form (pH 8.0) from the static measurement is also indicated (blue solid line).

Mutation effects against ESPT efficiency

To investigate the possible candidate(s) for proton acceptor after ESPT, the author utilized two mutants E46Q-coumarin and R52Q-coumarin. In native PYP system, both E46 and R52 are located near the chromophore (**Figure 2-1B**).

The absorption maxima measured at neutral pH 8.0 conditions were observed at 444, 442, and 452 nm for wtPYP-coumarin, R52Q-coumarin and E46Q-coumarin, respectively (**Figure 3-3**). Spectral changes upon lowering the pH and a clear isosbestic point at 403 or 407 nm (**Figure 3-4 and 3-5**) for R52Q-coumarin and E46Q-coumarin, respectively, indicate that the reaction is virtually a 2-state transition, similar with the wtPYP-coumarin.

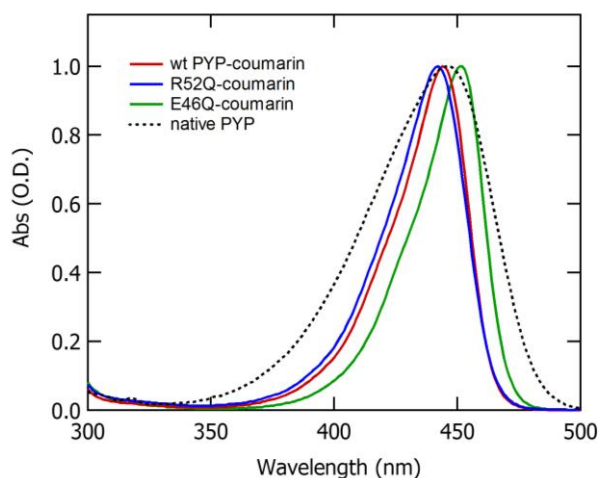


Figure 3-3. UV-Vis absorption spectra of wtPYP-coumarin (red), R52Q-coumarin (blue), E46Q-coumarin (green) and the intact PYP (dotted line) measured at pH 8.0. The buffer condition is 20 mM Tris HCl, RT.

Fluorescence emission and absorption spectra from the wtPYP-coumarin and two mutants were measured under two different pH conditions : neutral pH 8.0 and acidic pH 3.0. In neutral condition, the fluorescence maximum of PYP-coumarin, R52Q-coumarin, and E46Q-coumarin is at, respectively, 466, 467 and 473 nm (**Figure 3-3**). R52Q-coumarin shows a unique behavior of red-shifted emission with no respect to the transition wavelength in which it absorbs the light and thus has the largest Stokes shift compared to other reconstituted proteins. Moreover, R52Q-coumarin has the highest fluorescence efficiency (**Figure 3-6**) in the neutral condition, up to 3 times brighter than wtPYP-coumarin. Previous studies of native PYP have proposed the important role of R52 in the photochemistry reaction of PYP (71). Crystal structure of the mutant R52Q also demonstrates a role of R52 as a shield protector of the PYP chromophore from bulk water (35). Therefore, it is of great interest to study the protein-related solvation effects by mutating PYP-coumarin together with time-resolved profiles as well.

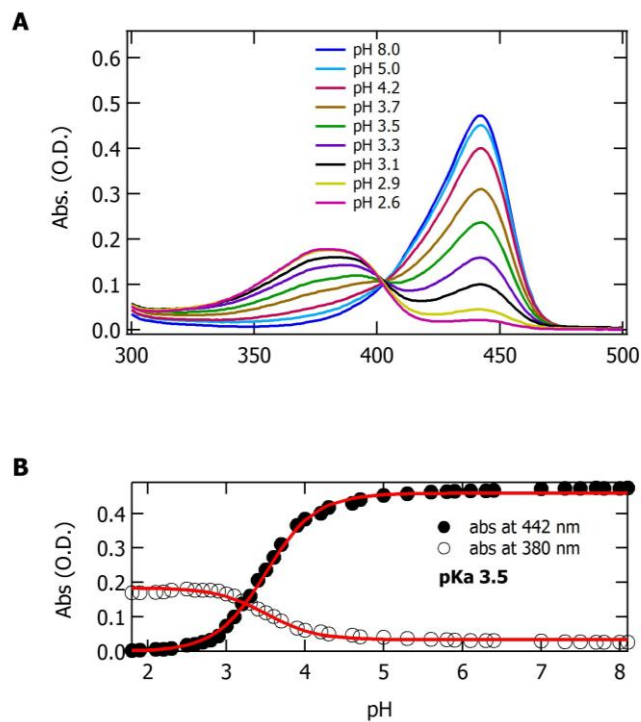


Figure 3-4. (A) UV-Visible absorption spectra of R52Q-coumarin measured at pH 8.0, 5.0, 4.2, 3.7, 3.5, 3.3, 3.1, 2.9 and 2.6. (B) Titration curves monitored at 442 nm (filled circle) and 380 nm (open circle). The buffer condition is 20 mM Tris HCl, RT.

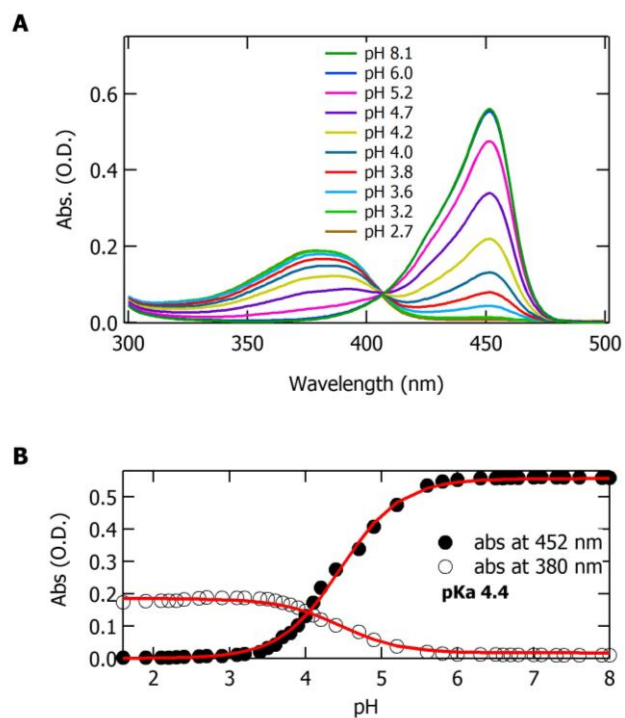


Figure 3-5. (A) UV-Visible absorption spectra of E46Q-coumarin measured at pH 8.1, 6.0, 5.2, 4.7, 4.2, 4.0, 3.8, 3.6, 3.2 and 2.7. (B) Titration curves monitored at 452 nm (filled circle) and 380 nm (open circle). The buffer condition is 20 mM Tris HCl, RT.

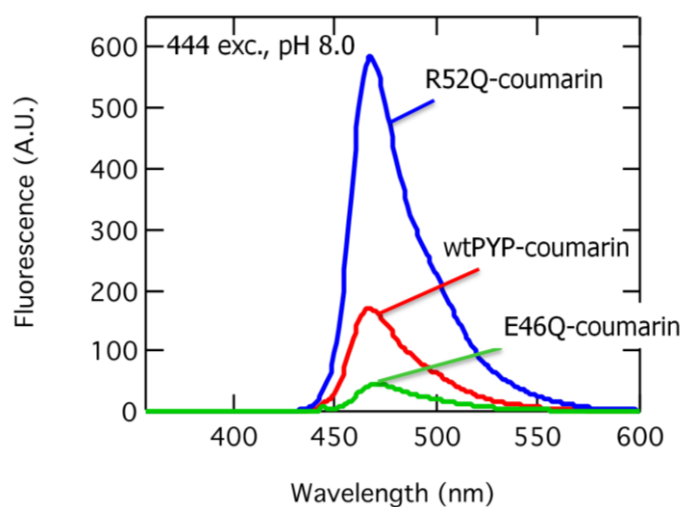


Figure 3-6. Emission spectra of wtPYP-coumarin (red), R52Q-coumarin (blue) and E46Q-coumarin (green) measured at neutral pH 8.0 under room temperature. Spectra were normalized using their absorption values at corresponding excitation wavelength used in the measurement. The buffer condition is 20 mM Tris HCl.

Figure 3-7 shows the emission spectra of two mutants at pH 3.0 and pH 3.5, compared to wtPYP-coumarin. All of the samples show double maxima, indicating ESPT occurrences, but the ESPT efficiency is different among these samples. WtPYP-coumarin shows that the deprotonated form emission has higher intensity than the protonated form at both pH 3.0 and 3.5. Mutant R52Q-coumarin shows high intensity of ESPT at pH 3.5, but lowering the pH to 3.0 resulting ESPT suppression. The pH-sensitive feature (between pH 3.0~3.5) of R52Q-coumarin could be a basis for designing such a local pH indicator. In the case of mutant E46Q-coumarin, the ESPT is highly suppressed both at pH 3.0 and 3.5. These observations suggest that point mutations against PYP-coumarin clearly influence the ESPT efficiency. This result indicates that alteration of hydrogen bonding network around the chromophore influence the ESPT.

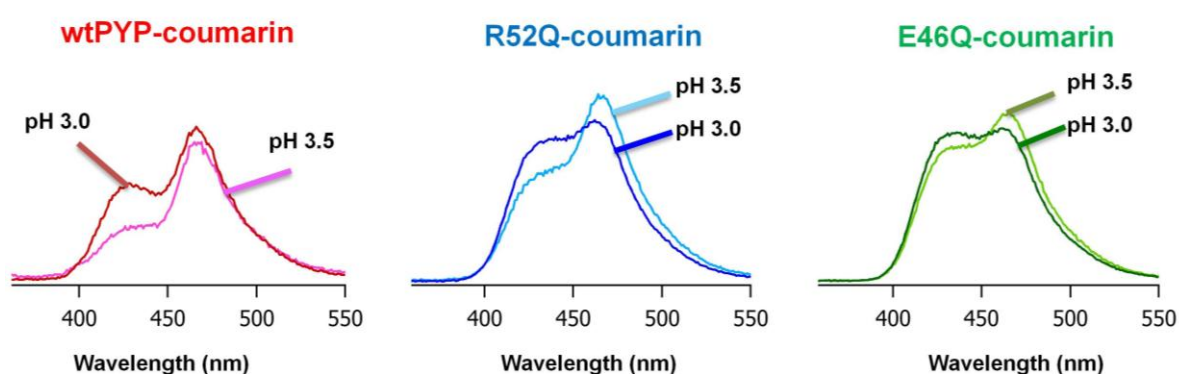


Figure 3-7. Emission spectra of wtPYP-coumarin (left panel), R52Q-coumarin (middle panel), and E46Q-coumarin (right panel) at pH 3.0 and 3.5. Excitation wavelength is 350 nm, in 20 mM Tris HCl, RT.

I normalized the emission spectra of the PYP-coumarin system at Figure 3-7 by the emission intensity value at 430 nm, shown by Figure 3.8. In this figure, ESPT efficiency among the samples at pH 3.0 can be easily compared. At this pH condition, wtPYP-coumarin shows the highest ESPT efficiency, while both mutants R52Q-coumarin and E46Q-coumarin suppress the ESPT efficiency. From this result, it can be proposed that possible candidates of proton acceptors might be E46 and R52.

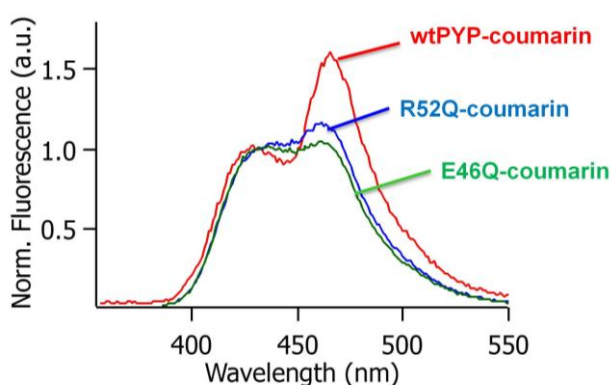


Figure 3.8. Normalized emission spectra of wtPYP-coumarin, R52Q-coumarin, and E46Q-coumarin by their emission value at 430 nm. Excitation wavelength is 350 nm, in 20 mM Tris HCl pH 3.0, RT.

In the master thesis document of Mr. M. Noji, he proposed that E46 of native PYP is deprotonated even at acidic pH. This proposal was based on the Fourier Transform Infra Red (FTIR) experiments (see **Appendix 2-3**) (72). According to the ordinary method to extract the IR band, sample is usually irradiated to trigger the photoreaction of PYP. In that result, difference in absorbance between light and dark conditions in IR region was obtained. The

observation he reported was at acidic pH condition. In the mutant R52Q (**Appendix 2**), a large negative band at 1771 cm^{-1} indicates the protonated E46. As a control, in the native PYP (**Appendix 3**), this negative band disappeared, so he proposed that E46 is deprotonated but pCA is protonated at acidic pH. At neutral condition, pCA is partially deprotonated (16). Therefore, his result suggested that acidic induced proton transfer occurs in native PYP (72). **Figure 3-9 (upper panel)** depicts protonation state of pCA and E46 in native PYP. If similar case can be applied to the PYP-coumarin system, then E46 might be also deprotonated even at acidic pH (**Figure 3-9B, bottom panel**). From this knowledge, the E46 is one possible candidate for proton acceptor at the excited state.

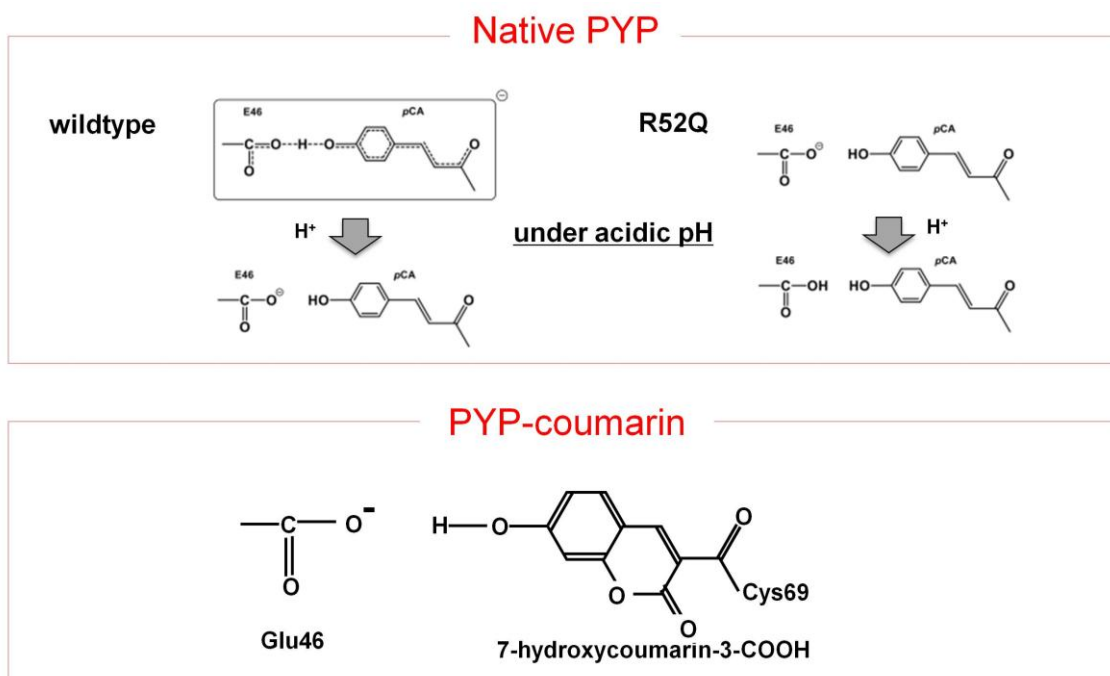


Figure 3-9. Protonation states of pCA and E46 in the native PYP and the mutant R52Q (upper panel). The proposed protonation state of E46 in the PYP-coumarin system (bottom panel). See text for detailed description.

Furthermore, I also investigated the mutation effects with the time-resolved fluorescence measurement. Since the pKa values of the reconstituted proteins used in this experiment are different, as described earlier, pH 3.0 was chosen as a moderate acidic pH value to compare the fluorescence properties using steady-state and time-resolved fluorescence measurements. On the other hand, pH 8.0 was selected to represent the neutral deprotonated condition. The TCSPC measurements were carried out in two pH conditions : wtPYP-coumarin, R52Q-coumarin, and E46Q-coumarin at neutral pH 8.0, with $\lambda_{ex}= 444$ nm, and at acidic pH 3.0, with $\lambda_{ex}= 365$ nm. In order to obtain the spectral evolution as time progress, the author analyzed the lifetime decay using global analysis.

The fluorescence emission decay curves together with the fitting functions obtained from the TCSPC measurements for the wtPYP-coumarin, R52Q-coumarin and E46Q-coumarin can be seen in the **Figure 3-10~3-15**. The results of the fits and corresponding time constants are presented in Table 3-1. As with the first acidic sample measured (wtPYP-coumarin pH 2.1), the faster fluorescence decay can be attributed to the relaxation of the protonated form excited state, while the second decay component is associated to the deprotonated form relaxation. Based on **Table 3-1**, at acidic condition, the fluorescence emission decay for all samples seems essentially double exponential. Spectral components of wtPYP-coumarin, the mutants R52Q-coumarin and E46Q-coumarin show similar behaviors. This indicates that they possess similar photochemistry. Therefore, the

difference is in the ESPT efficiency as described previously.

In general, at such acidic pH conditions (pH 3.0), the tertiary structure of a protein is highly destabilized. However, the tertiary structure of PYP is well known to be stable under these pH conditions. To examine the stability of the tertiary structure of the PYP-coumarin as well as the mutants, circular dichroism (CD) spectra were measured at neutral and acidic pH (see Appendix 1). The CD spectrum is usually used to examine the secondary structure formation of proteins. The CD spectrum of wtPYP-coumarin at pH 8.0 is almost identical to that of native PYP, indicating that the binding of coumarin never affects the tertiary structure of PYP. Furthermore, the spectrum at the acidic condition (pH 3.0) still shows large ellipticity compared to that at the neutral pH, indicating that PYP-coumarin also remains to be native-like structure even at the acidic pH. Unfortunately, at this stage, the author does not have any information about the detailed molar extinction of wtPYP-coumarin and the mutants, thus their CD spectra cannot be compared each other directly.

On the contrary, the situation in the neutral pH (pH 8.0) is somewhat different. Under this condition, mutant R52Q-coumarin shows prominent difference in the slow component. Moreover, the mutant E46Q-coumarin almost no signal found in the 20 ns time scale measurement. Generally, the lifetimes of the deprotonated state from the protonated state after ESPT is longer than that of the deprotonated state at neutral pH. This lifetime might reflect the chromophore environment. However, in the neutral condition, the deprotonated

chromophore of wtPYP-coumarin and E46Q-coumarin shows faster lifetime than R52Q-coumarin. Only in the R52Q-coumarin, the obtained time constants shows substantial amount of slower component. Therefore, the author expects that the result of R52Q-coumarin is helpful to investigate this problem. The fact that only R52Q-coumarin which shows high amount of slow component leads the author to assume that hydrogen bonding network of R52Q-coumarin might be close to the hydrogen bonding network of wtPYP-coumarin in acidic condition after ESPT. To trace the proton pathway after ESPT is a difficult task without any detailed structural information of the PYP-coumarin. Since E46 of native PYP was indicated to be deprotonated even at acidic condition (72), the author proposed that E46 of PYP-coumarin might be also deprotonated even at acidic condition. The deprotonated E46 is one of the candidates of proton acceptor from coumarin analogue at the excited state. However, the ESPT still remains in the mutant E46Q-coumarin as shown on the earlier fluorescence properties. Therefore, the author proposed two possible proton transfer pathways. One is to the deprotonated E46, and the other is to an unknown acceptor, or direct release to aqueous milieu.

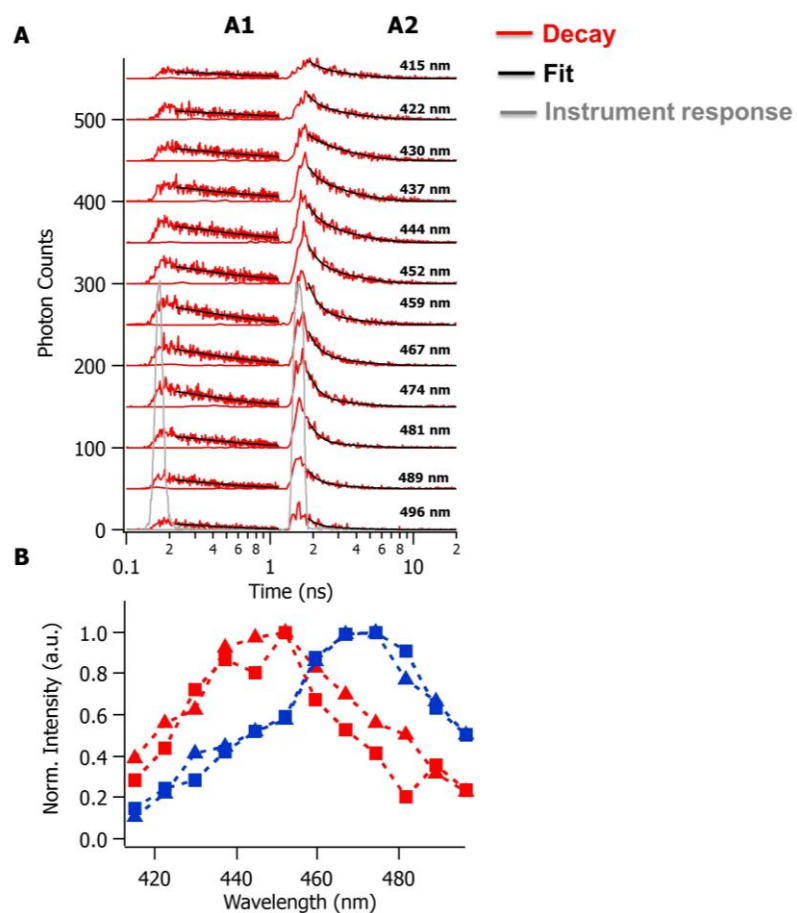


Figure 3-10. (A) Fluorescence emission decay curves (red lines) of wtPYP-coumarin at pH 3.0 fitted using global analysis with double exponential functions. Excitation wavelength is 365 nm, with time window 1 ns (A1 panel) and 20 ns (A2 panel). The black lines indicate the fitted curves, and the grey line shows the instrumental response. B. Reconstructed spectral component obtained by analyzing the decay with double-exponential function using global analysis, normalized to the same intensity value (see Appendix 4 for details). Fast and slow fluorescence components are shown by red and blue dotted lines, respectively, for both 1 ns (cross) and 20 ns (triangle) time windows.

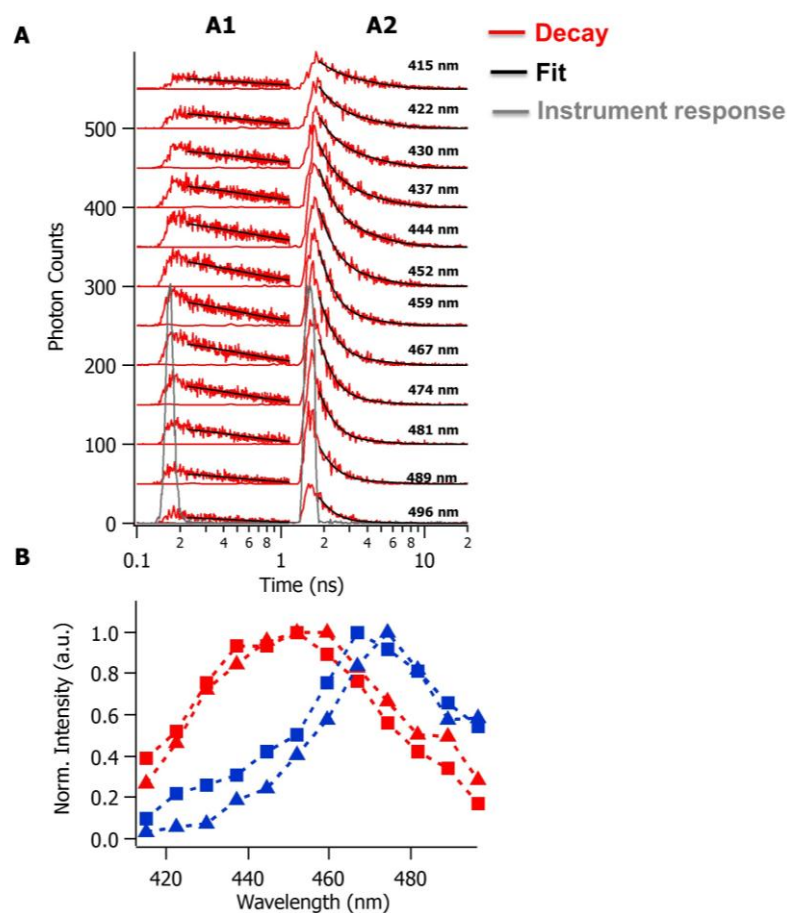


Figure 3-11. (A) Fluorescence emission decay curves (red lines) of R52Q-coumarin at pH 3.0 fitted using global analysis with double exponential functions. Excitation wavelength is 365 nm, with time window 1 ns (A1 panel) and 20 ns (A2 panel). The black lines indicate the fitted curves, and the grey line shows the instrumental response. (B) Reconstructed spectral components obtained by analyzing the decay with double-exponential function using global analysis, normalized to the same intensity value (see Appendix 4 for details). Fast and slow fluorescence components are shown by red and blue dotted lines, respectively, for both 1 ns (triangle) and 20 ns (square) time windows.

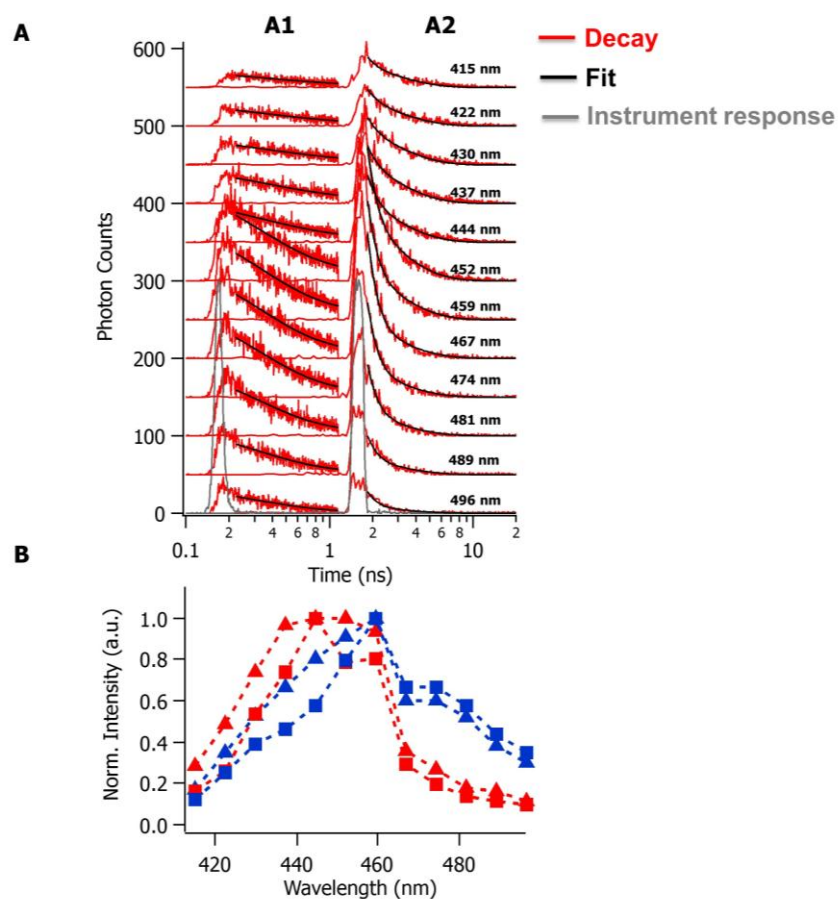


Figure 3-12. (A) Fluorescence emission decay curves (red lines) of E46Q-coumarin at pH 3.0 fitted using global analysis with double exponential functions. Excitation wavelength is 365 nm, with time window 1 ns (A1 panel) and 20 ns (A2 panel). The black lines indicate the fitted curves, and the grey line shows the instrumental response. (B) Reconstructed spectral component obtained by analyzing the decay with double-exponential functions using global analysis, normalized to the same intensity value (see Appendix 4 for details). Fast and slow fluorescence components are shown by red and blue dotted lines, respectively, for both 1 ns (triangle) and 20 ns (square) time windows.

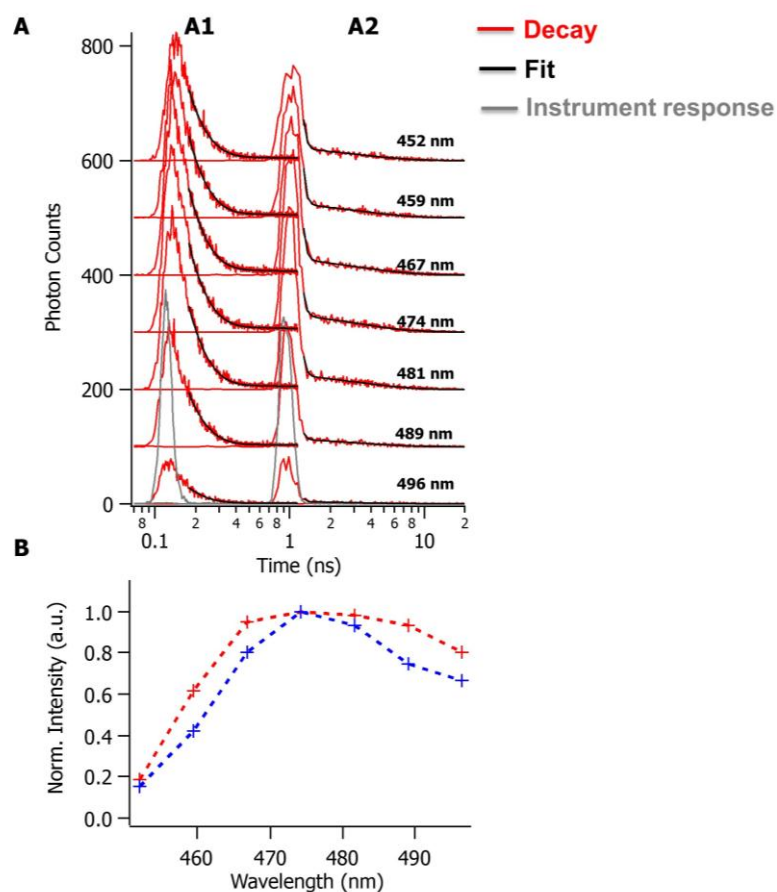


Figure 3-13. (A) Fluorescence emission decay curves (red lines) of wtPYP-coumarin at pH 8.0 fitted using global analysis with double exponential functions. Excitation wavelength is 444 nm, with time window 1 ns (A1 panel) and 20 ns (A2 panel). The black lines indicate the fitted curves, and the grey line shows the instrumental response. (B) Reconstructed spectral components obtained by analyzing the decay with double-exponential functions using global analysis, normalized to the same intensity value (see Appendix 4 for details). Fast and slow fluorescence components of 1 ns time window measurement are shown by red and blue dotted lines, respectively.

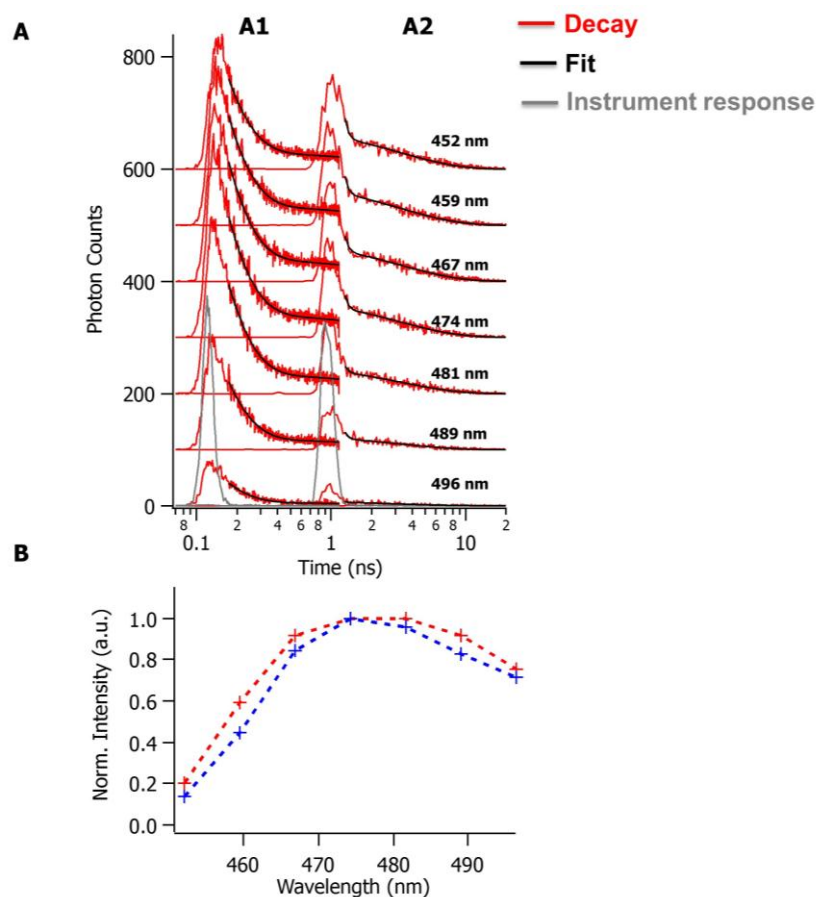


Figure 3-14. (A) Fluorescence emission decay curves (red lines) of R52Q-coumarin at pH 8.0 fitted using global analysis with double exponential functions. Excitation wavelength is 444 nm, with time window 1 ns (A1 panel) and 20 ns (A2 panel). The black lines indicate the fitted curves, and the grey line shows the instrumental response. (B) Reconstructed spectral components obtained by analyzing the decay with double-exponential functions using global analysis, normalized to the same intensity value (see Appendix 4 for details). Fast and slow fluorescence components of 1 ns time window measurement are shown by red and blue dotted lines, respectively.

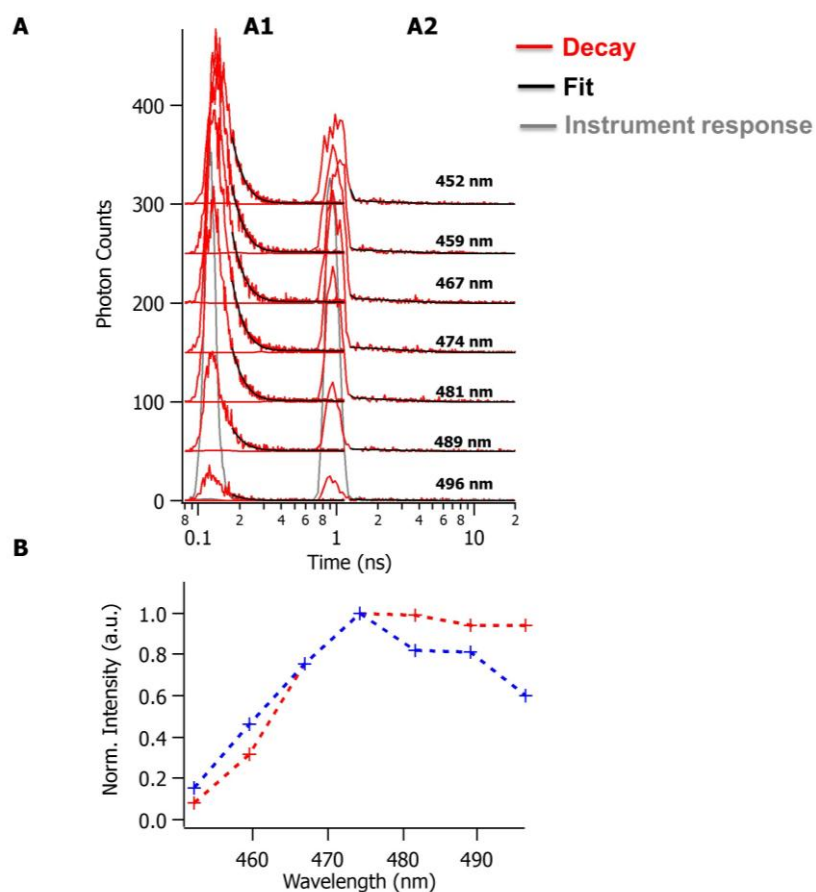


Figure 3-15. (A) Fluorescence emission decay curves (red lines) of E46Q-coumarin at pH 8.0 fitted using global analysis with double exponential functions. Excitation wavelength is 444 nm, with time window 1 ns (A1 panel) and 20 ns (A2 panel). The black lines indicate the fitted curves, and the grey line shows the instrumental response. (B) Reconstructed spectral components obtained by analyzing the decay with double-exponential functions using global analysis, normalized to the same intensity value (see Appendix 4 for details). Fast and slow fluorescence components of 1 ns time window measurement are shown by red and blue dotted lines, respectively.

Table 3-1.

Time constants (τ_i) obtained from global analysis of fluorescence decays of the PYP-coumarin and two mutants R52Q-coumarin and E46Q-coumarin, measured by time-correlated single photon counting technique using time windows 1 and 20 ns, with excitation wavelength at 444 and 365 nm for each neutral and acidic condition.

System	Neutral pH 8.0, 444 nm exc.		Acidic pH 3.0, 365 nm exc.	
	τ_1	τ_2	τ_1	τ_2
wtPYP-coumarin	0.063 ns (0.94)	3.131 ns (0.06)	0.318±0.010 ns	2.160±0.004 ns
(acidic pH 2.1)	-	-	0.383±0.007 ns	2.336±0.029 ns
R52Q-coumarin	0.079 ns (0.79)	3.329 ns (0.20)	0.497±0.008 ns	2.525±0.050 ns
E46Q-coumarin	0.039 ns (0.99)	2.218 ns (0.01)	0.297±0.005 ns	1.792±0.030 ns

Chapter 4. General Conclusion

In this study, the poorly fluorescent photoactive yellow protein has been modified to emit strong fluorescence by covalently attaching to *trans*-locked pCA, 7-hydroxycoumarin-3-carboxylic acid. The formation of hydrogen bonding network in the reconstituted protein is confirmed by the similar behavior of spectral changes upon lowering the pH, and the same pKa value between the PYP-coumarin and native PYP. The protonated PYP-coumarin showed a bilobed emission spectrum, where the λ_{max} correlated well with that of the deprotonated PYP-coumarin. The fact indicates that ESPT occurs in PYP-coumarin, and implies that the hydrogen-bond network mediates the ESPT. From the time-resolved fluorescence measurement based on streak camera detection using TCSPC technique, the author succeeded in identifying two spectral components with independent time constants and λ_{max} of 437 nm and 468 nm. The existence of these fast and slow emission spectra leads to the conclusion that there are two independent excited states and that they have different decay times. These two spectral components confirmed the composition of bilobed shape spectrum at acidic pH obtained from the static measurement. Therefore, there is no direct evidence to obtain the rate of the ESPT since ESPT has already occurred at this time region. Furthermore, the fluorescence properties of the two mutants R52Q-coumarin and E46Q-coumarin revealed that these two mutations influence the efficiency of the ESPT. At acidic pH, the fact that mutant E46Q-coumarin highly suppresses the ESPT efficiency is

useful to identify the proton acceptor after ESPT at the excited state. The protonation state of E46 and the hydrogen bond between the E46 with the chromophore affect the ESPT efficiency in protonated PYP-coumarin, indicating that the hydrogen bonding network mediates ESPT.

These results suggest a new viewpoint toward photoreaction of PYP. The importance of hydrogen-bond network has become a contemporary research interest because its main specific interaction is central to understand microscopic structures and functions in many molecular systems. Recent theoretical studies using mixed quantum/classical (QM/MM) MD simulation technique against PYP (73) and GFP (74, 75) chromophore also suggest that hydrogen-bond interactions and solvent stabilization provide a general mechanism for excited state decay of chromophore in solution. Nevertheless, these experiments are still ongoing and promise to provide even more intricate detail through more sophisticated time-resolved emission and X-ray diffraction experiments. The crystallization condition has already been found, and preliminary small crystals have been obtained (**Figure 4.1**). In the future, based on the crystal structure of PYP-coumarin, the precise mechanism of ESPT within the protein will be revealed.

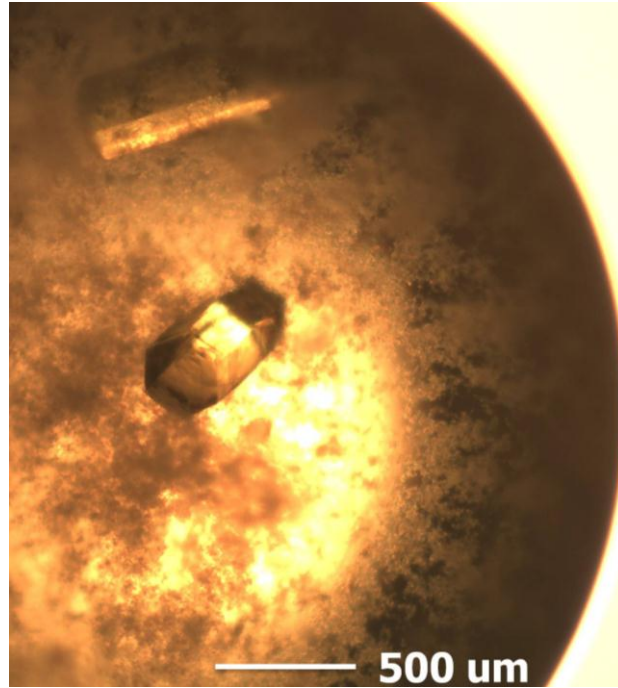


Figure 4-1. Crystals of wtPYP-coumarin grown with a PYP-concentration of $10 \text{ mg}\cdot\text{ml}^{-1}$ in a drop with a precipitant of 2.2 M ammonium sulfate with 1.2 M sodium chloride. Temperature and pH are 293 K and pH 9.0, respectively.

Acknowledgments

First of all, I am grateful to the Almighty God, Allah SWT for the wisdom that He has been bestowed upon me during the doctoral research, and indeed, throughout my life. I would like to express my sincere gratitude to my academic supervisor, Professor Mikio Kataoka, for providing an opportunity to work in his group, his support, regular guidance and encouragement during the course of my Ph. D. work.

I am deeply grateful to Professor Hironari Kamikubo for suggesting the experimental work and the regular guidance of this work from the very beginning to the ending of the project, as well as his painstaking effort in proofreading the thesis and paper draft, are greatly appreciated.

I would like to express my gratitude to my supervisor committee, Professor Tsuyoshi Kawai and Professor Takashi Matsuo for their insightful comments and valuable suggestions.

My special thanks to Professor Yoichi Yamazaki and Dr. Mariko Yamaguchi for their support, guidance, advice throughout the doctoral research. Dr. Mariko Yamaguchi gave so much help during the analysis of the lifetime fluorescence.

I would like to express the deepest appreciation the Global Center of Excellent (COE) Program for providing the fellowship to carry out this research and to my former supervisors Professor Kuwat Triyana, Professor Nastiti Wijayanti and Professor Eko Tri Sulistya for giving me a recommendation to pursue the doctoral degree in Japan.

I also take this opportunity to record my sincere thanks to all members of Bioenergetics and Biophysics Laboratory for their support, friendship and warm encouragement. Special thanks to Ms. Satomi Kayamura who prepared the PYP plasmids in the laboratory. I also greatly appreciate the help of Mr. Yasuo Okajima during the lifetime fluorescence experiments. My time here would have been immeasurably more difficult without the help of Ms. Yuko Fujisawa, Ms. Mayumi Mizutani, and the staff of NAIST Student Affair Section who deliver the important information and assist the daily life.

Finally, I am thankful to my husband Mohammad Nur Hasan for his love and continuous support and my son Rizqi Haikal Hasan who always reduce my tiredness when I returned from work. This small work is dedicated to my parents for their unconditional encouragement, pray and support throughout my life and also for my late brother and sister, Dani and Dina.

List of publications

Publication

Excited-State Proton Transfer in Fluorescent Photoactive Yellow Protein Containing
7-Hydroxycoumarin

Dian Novitasari, Hironari Kamikubo, Yoichi Yamazaki, Mariko Yamaguchi, and Mikio

Kataoka, *Advanced Materials Research* Vol. 896 (2014), 85-88, DOI :

10.4028/www.scientific.net/AMR.896.85.

Conferences

1. Fluorescence properties of chromophore-modified Photoactive Yellow Protein

Dian Novitasari, Hironari Kamikubo, Yoichi Yamazaki, Mariko Yamaguchi, and Mikio

Kataoka

The 6th International Symposium on Molecular Science of Fluctuations toward
Biological Functions, Kyoto, November, 2012 (Poster Presentation).

2. Excited-state proton transfer of fluorescent Photoactive Yellow Protein containing
7-hydroxycoumarin

Dian Novitasari, Hironari Kamikubo, Yoichi Yamazaki, Mariko Yamaguchi, and Mikio

Kataoka

The 2013 International Conference on Advanced Materials Science and Technology,
Yogyakarta, Indonesia, September 2013 (Oral Presentation).

3. Excited-state proton transfer of fluorescent Photoactive Yellow Protein reconstituted with hydroxycoumarin

Dian Novitasari, Hironari Kamikubo, Yoichi Yamazaki, Mariko Yamaguchi, and Mikio Kataoka

The 51st Annual meeting of The Biophysical Society of Japan, Kyoto, October 2013 (Poster Presentation).

4. Excited-state proton transfer of fluorescent Photoactive Yellow Protein containing 7-hydroxycoumarin

Dian Novitasari, Hironari Kamikubo, Yoichi Yamazaki, Mariko Yamaguchi, and Mikio Kataoka

The 2013 GIST-NCTU- NAIST International Joint Symposium on Innovative Materials for Future Technology, Nara, Japan, November 2013 (Oral Presentation).

References

1. Gilman, A. G. (1987) G proteins: transducers of receptor-generated signals, *Annual review of biochemistry* 56, 615-649.
2. Meyer, T. E. (1985) Isolation and characterization of soluble cytochromes, ferredoxins and other chromophoric proteins from the halophilic phototrophic bacterium *Ectothiorhodospira halophila*, *Biochimica et biophysica acta* 806, 175-183.
3. Meyer, T. E., Yakali, E., Cusanovich, M. A., Tollin, G. (1987) Properties of a water-soluble, yellow protein isolated from a halophilic phototrophic bacterium that has photochemical activity analogous to sensory rhodopsin, *Biochemistry* 26, 418-423.
4. Bogomolni, R. A., Spudich, J. L. (1982) Identification of a third rhodopsin-like pigment in phototactic *Halobacterium halobium*, *Proceedings of the National Academy of Sciences of the United States of America* 79, 6250-6254.
5. Van Beeumen, J. J., Devreese, B. V., Van Bun, S. M., Hoff, W. D., Hellingwerf, K. J., Meyer, T. E., McRee, D. E., Cusanovich, M. A. (1993) Primary structure of a photoactive yellow protein from the phototrophic bacterium *Ectothiorhodospira halophila*, with evidence for the mass and the binding site of the chromophore, *Protein Science* 2, 1114-1125.
6. Sprenger, W. W., Hoff, W. D., Armitage, J. P., and Hellingwerf, K. J. (1993) The

- eubacterium *Ectothiorhodospira halophila* is negatively phototactic, with a wavelength dependence that fits the absorption spectrum of the photoactive yellow protein, *Journal of Bacteriology* 175, 3096-3104.
7. Borgstahl, G. E., Williams, D. R., Getzoff, E. D. (1995) 1.4 Å structure of photoactive yellow protein, a cytosolic photoreceptor: unusual fold, active site, and chromophore, *Biochemistry* 34, 6278-6287.
 8. Pellequer, J. L., Wager-Smith, K. A., Kay, S. A., Getzoff, E. D. (1998) Photoactive yellow protein: a structural prototype for the three-dimensional fold of the PAS domain superfamily, *Proceedings of the National Academy of Sciences of the United States of America* 95, 5884-5890.
 9. Imamoto, Y., Kataoka, M. (2007) Structure and photoreaction of photoactive yellow protein, a structural prototype of the PAS domain superfamily, *Photochemistry and Photobiology* 83, 40-49.
 10. Ng, K., Getzoff, E. D., Moffat, K. (1995) Optical studies of a bacterial photoreceptor protein, photoactive yellow protein, in single crystals, *Biochemistry* 34, 879-890.
 11. Hoff, W. D., Kwa, S. L. S., van Grondelle, R., Hellingwerf, K. J. (1992) Low Temperature Absorbance and Fluorescence Spectroscopy of the Photoactive Yellow Protein from *Ectothiorhodospira halophila*, *Photochemistry and Photobiology* 56, 529-539.

12. Cusanovich, M. A., Meyer, T. E. (2003) Photoactive yellow protein: a prototypic PAS domain sensory protein and development of a common signaling mechanism, *Biochemistry* 42, 4759-4770.
13. Meyer, T. E., Tollin, G., Hazzard, J. H., Cusanovich, M. A. (1989) Photoactive yellow protein from the purple phototrophic bacterium, *Ectothiorhodospira halophila*. Quantum yield of photobleaching and effects of temperature, alcohols, glycerol, and sucrose on kinetics of photobleaching and recovery, *Biophysical Journal* 56, 559-564.
14. Griesbeck, A., Oelgemöller, M., Ghetti, F. (2012) *CRC Handbook of Organic Photochemistry and Photobiology*, Vol. 1.
15. Anderson, S., Crosson, S., Moffat, K. (2004) Short hydrogen bonds in photoactive yellow protein, *Acta crystallographica Section D, Biological crystallography* 60, 1008-1016.
16. Yamaguchi, S., Kamikubo, H., Kurihara, K., Kuroki, R., Niimura, N., Shimizu, N., Yamazaki, Y., Kataoka, M. (2009) Low-barrier hydrogen bond in photoactive yellow protein, *Proceedings of the National Academy of Sciences of the United States of America* 106, 440-444.
17. Sigala, P. A., Tsuchida, M. A., Herschlag, D. (2009) Hydrogen bond dynamics in the active site of photoactive yellow protein, *Proceedings of the National Academy of Sciences of the United States of America* 106, 9232-9237.

18. Schotte, F., Cho, H. S., Kaila, V. R. I., Kamikubo, H., Dashdorj, N., Henry, E. R., Graber, T. J., Henning, R., Wulff, M., Hummer, G., Kataoka, M., Anfinrud, P. A. . (2012) Watching a signaling protein function in real time via 100-ps time-resolved Laue crystallography, *Proceedings of the National Academy of Sciences of the United States of America* 109, 19256-19261.
19. Ujj, L., Devanathan, S., Meyer, T. E., Cusanovich, M. A., Tollin, G., Atkinson, G. H. (1998) New photocycle intermediates in the photoactive yellow protein from *Ectothiorhodospira halophila*: picosecond transient absorption spectroscopy, *Biophysical Journal* 75, 406-412.
20. Devanathan, S., Pacheco, A., Ujj, L., Cusanovich, M., Tollin, G., Lin, S., Woodbury, N. (1999) Femtosecond spectroscopic observations of initial intermediates in the photocycle of the photoactive yellow protein from *Ectothiorhodospira halophila*, *Biophysical Journal* 77, 1017-1023.
21. Meyer, T. E., Tollin, G., Causgrove, T. P., Cheng, P., Blankenship, R. E. (1991) Picosecond decay kinetics and quantum yield of fluorescence of the photoactive yellow protein from the halophilic purple phototrophic bacterium, *Ectothiorhodospira halophila*, *Biophysical Journal* 59, 988-991.
22. Kroon, A. R., Hoff, W. D., Fennema, H. P., Gijzen, J., Koomen, G. J., Verhoeven, J. W., Crielaard, W., Hellingwerf, K. J. (1996) Spectral tuning, fluorescence, and

- photoactivity in hybrids of photoactive yellow protein, reconstituted with native or modified chromophores, *Journal of Biological Chemistry* 271, 31949-31956.
23. Mihara, K., Hisatomi, O., Imamoto, Y., Kataoka, M., Tokunaga, F. (1997) Functional expression and site-directed mutagenesis of photoactive yellow protein, *Journal of Biochemistry* 121, 876-880.
 24. Brudler, R., Meyer, T. E., Genick, U. K., Devanathan, S., Woo, T. T., Millar, D. P., Gerwert, K., Cusanovich, M. A., Tollin, G., Getzoff, E. D. (2000) Coupling of hydrogen bonding to chromophore conformation and function in photoactive yellow protein, *Biochemistry* 39, 13478-13486.
 25. Demchuk, E., Genick, U. K., Woo, T. T., Getzoff, E. D., Bashford, D. (2000) Protonation states and pH titration in the photocycle of photoactive yellow protein, *Biochemistry* 39, 1100-1113.
 26. Devanathan, S., Lin, S., Cusanovich, M. A., Woodbury, N., Tollin, G. (2001) Early photocycle kinetic behavior of the E46A and Y42F mutants of photoactive yellow protein: femtosecond spectroscopy, *Biophysical Journal* 81, 2314-2319.
 27. Imamoto, Y., Koshimizu, H., Mihara, K., Hisatomi, O., Mizukami, T., Tsujimoto, K., Kataoka, M., Tokunaga, F. (2001) Roles of amino acid residues near the chromophore of photoactive yellow protein, *Biochemistry* 40, 4679-4685.
 28. Devanathan, S., Brudler, R., Hessling, B., Woo, T. T., Gerwert, K., Getzoff, E. D.,

- Cusanovich, M. A., Tollin, G. (1999) Dual photoactive species in Glu46Asp and Glu46Ala mutants of photoactive yellow protein: a pH-driven color transition, *Biochemistry* 38, 13766-13772.
29. Devanathan, S., Lin, S., Cusanovich, M. A., Woodbury, N., Tollin, G. (2000) Early intermediates in the photocycle of the Glu46Gln mutant of photoactive yellow protein: femtosecond spectroscopy, *Biophysical Journal* 79, 2132-2137.
30. Imamoto, Y., Mihara, K., Hisatomi, O., Kataoka, M., Tokunaga, F., Bojkova, N., Yoshihara, K. (1997) Evidence for proton transfer from Glu-46 to the chromophore during the photocycle of photoactive yellow protein, *Journal of Biological Chemistry* 272, 12905-12908.
31. Genick, U. K., Devanathan, S., Meyer, T. E., Canestrelli, I. L., Williams, E., Cusanovich, M. A., Tollin, G., Getzoff, E. D. (1997) Active site mutants implicate key residues for control of color and light cycle kinetics of photoactive yellow protein, *Biochemistry* 36, 8-14.
32. Philip, A. F., Nome, R. A., Papadantonakis, G. A., Scherer, N. F., Hoff, W. D. (2010) Spectral tuning in photoactive yellow protein by modulation of the shape of the excited state energy surface, *Proceedings of the National Academy of Sciences of the United States of America* 107, 5821-5826.
33. van Aalten, D. M., Haker, A., Hendriks, J., Hellingwerf, K. J., Joshua-Tor, L.,

- Crielaard, W. (2002) Engineering photocycle dynamics. Crystal structures and kinetics of three photoactive yellow protein hinge-bending mutants, *Journal of Biological Chemistry* 277, 6463-6468.
34. Mataga N., C. H., Shibata Y., Imamoto Y., Kataoka M., Tokunaga F. (2002) Ultrafast photoinduced reaction dynamics of photoactive yellow protein (PYP): observation of coherent oscillations in the femtosecond fluorescence decay dynamics, *Chemical Physics Letter* 352, 220-225.
35. Shimizu, N., Kamikubo, H., Yamazaki, Y., Imamoto, Y., Kataoka, M. (2006) The crystal structure of the R52Q mutant demonstrates a role for R52 in chromophore pKa regulation in photoactive yellow protein, *Biochemistry* 45, 3542-3547.
36. Takeshita, K., Imamoto, Y., Kataoka, M., Mihara, K., Tokunaga, F., Terazima, M. (2002) Structural change of site-directed mutants of PYP: new dynamics during pR state, *Biophysical Journal* 83, 1567-1577.
37. Devanathan, S., Genick, U. K., Canestrelli, I. L., Meyer, T. E., Cusanovich, M. A., Getzoff, E. D., Tollin, G. (1998) New insights into the photocycle of *Ectothiorhodospira halophila* photoactive yellow protein: photorecovery of the long-lived photobleached intermediate in the Met100Ala mutant, *Biochemistry* 37, 11563-11568.
38. Kumauchi, M., Hamada, N., Sasaki, J., Tokunaga, F. (2002) A Role of

- Methionine100 in Facilitating PYP(M)-Decay Process in the Photocycle of Photoactive Yellow Protein, *The Journal of Biochemistry* 132, 205-210.
39. Hendriks, J., Hoff, W. D., Crielaard, W., Hellingwerf, K. J. (1999) Protonation/deprotonation reactions triggered by photoactivation of photoactive yellow protein from *Ectothiorhodospira halophila*, *Journal of Biological Chemistry* 274, 17655-17660.
40. van der Horst, M. A., van Stokkum, I. H., Crielaard, W., Hellingwerf, K. J. (2001) The role of the N-terminal domain of photoactive yellow protein in the transient partial unfolding during signalling state formation, *Febs Letters* 497, 26-30.
41. Baca, M., Borgstahl, G. E., Boissinot, M., Burke, P. M., Williams, D. R., Slater, K. A., Getzoff, E. D. (1994) Complete chemical structure of photoactive yellow protein: novel thioester-linked 4-hydroxycinnamyl chromophore and photocycle chemistry, *Biochemistry* 33, 14369-14377.
42. Cordfunke, R., Kort, R., Pierik, A., Gobets, B., Koomen, G. J., Verhoeven, J. W., Hellingwerf, K. J. (1998) Trans/cis (Z/E) photoisomerization of the chromophore of photoactive yellow protein is not a prerequisite for the initiation of the photocycle of this photoreceptor protein, *Proceedings of National Academy of Sciences of the United States of America* 95, 7396-7401.
43. van der Horst, M. A., Arents, J. C., Kort, R., Hellingwerf, K. J. (2007) Binding,

- tuning and mechanical function of the 4-hydroxy-cinnamic acid chromophore in photoactive yellow protein, *Photochemical and Photobiological Science* 6, 571-579.
44. Imamoto, Y., Shirahige, Y., Tokunaga, F., Kinoshita, T., Yoshihara, K., Kataoka, M. (2001) Low-temperature Fourier transform infrared spectroscopy of photoactive yellow protein, *Biochemistry* 40, 8997-9004.
45. Unno M., K. M., Sasaki J., Tokunaga F., Yamauchi S. (2002) Resonance Raman spectroscopy and quantum chemical calculations reveal structural changes in the active site of photoactive yellow protein, *Biochemistry* 41, 5668-5674.
46. Espagne, A., Paik, D. H., Chaugenet-Barret, P., Plaza, P., Martin, M. M., Zewail, A. H. (2007) Ultrafast light-induced response of photoactive yellow protein chromophore analogues, *Photochemical & photobiological sciences : Official journal of the European Photochemistry Association and the European Society for Photobiology* 6, 780-787.
47. Cody, C. W., Prasher, D. C., Westler, W. M., Prendergast, F. G., Ward, W. W. (1993) Chemical structure of the hexapeptide chromophore of the *Aequorea* green-fluorescent protein, *Biochemistry* 32, 1212-1218.
48. Loening, A. M., Fenn, T. D., Gambhir, S. S. (2007) Crystal structure of the luciferase and green fluorescent protein from *Renilla reniformis*, *Journal of Molecular Biology* 374, 1017-1028.

49. Morise, H., Shimomura, O., Johnson, F. H., Winant, J. (1974) Intermolecular energy transfer in bioluminescent system of *Aequorea*, *Biochemistry* 13, 2656-2662.
50. Underwood, T. J., Tallamy, D. W., Pesek, J. D. (1997) Bioluminescence in firefly larvae : a test of the aposematic display hypothesis (Coleoptera: Lampyridae), *Journal of Insect Behaviour* 10, 365-370.
51. Salih, A., Larkum, A., Cox, G., Kuhl, M., Hoegh-Guldberg, O. (2000) Fluorescent pigments in corals are photoprotective, *Nature* 408, 850-853.
52. Chudakov, D. M., Lukyanov, S., Lukyanov, K. A. (2005) Fluorescent proteins as a toolkit for *in vivo* imaging, *Trends in Biotechnology* 23, 605-613.
53. Tsien, R. Y. (1998) The Green Fluorescent Protein, *Annual Reviews of Biochemistry* 67, 509-544.
54. Ormo, M., Cubitt, A. B. , Kallio, K., Gross, L. A., Tsien, R. Y., Remington, S. J. (1996) Crystal structure of the *Aequorea victoria* Green Fluorescent Protein, *Science* 273, 1392-1395.
55. Pedelacq, J., Cabantous, S., Tran, T., Terwilliger, T. C., Waldo, G. S. (2006) Engineering and characterization of a superfolder green fluorescent protein, *Nature Biotechnology* 24, 79-88.
56. Yang, F., Moss, L. G., Phillips Jr., G. N. (1996) The molecular structure of green fluorescent protein, *Nature Biotechnology* 14, 1246-1251.

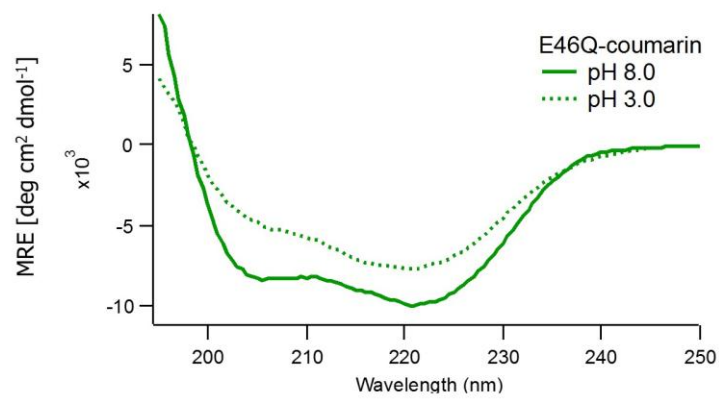
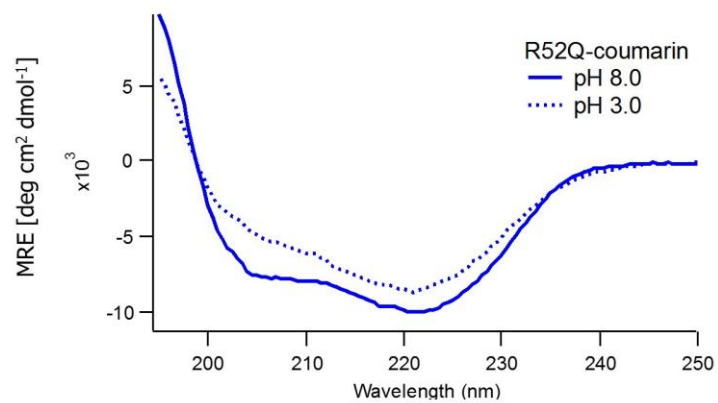
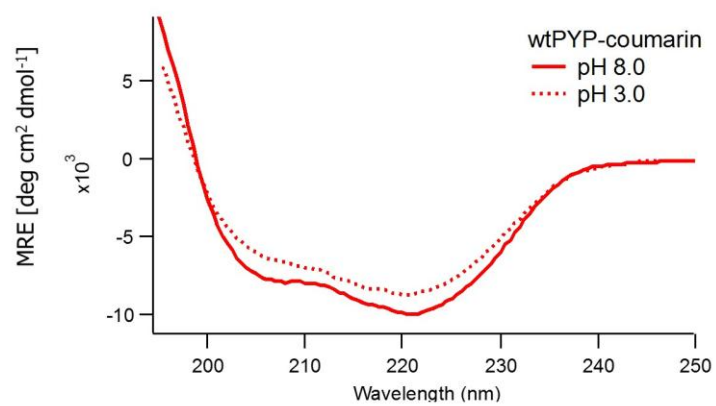
57. Cubitt, A. B., Heim, R., Adams, S. R., Boyd, A. E., Grossm, L. A., Tsien, R. Y. (1995) Understanding, improving and using green fluorescent protein, *Trends in Biochemical Science* 20, 448-455.
58. Heim, R., Tsien, R. Y. (1996) Engineering green fluorescent protein for improved brightness, longer wavelengths and fluorescence resonance energy transfer, *Current Biology* 6, 178-182.
59. Pan, Y. A., Livet, J., Sanes, J. R., Lichtman, J. W., Schier, A. F. (2011) Multicolor Brainbow imaging in zebrafish, *Cold Spring Harbor protocols 2011*, pdb.prot5546.
60. Weissman, T. A., Sanes, J. R., Lichtman, J. W., Livet, J. (2011) Generating and imaging multicolor Brainbow mice, *Cold Spring Harbor protocols 2011*, 763-769.
61. Chattoraj, M., King, B. A., Bublitz, G. U., Boxer, S. G. (1996) Ultra-fast excited state dynamics in green fluorescent protein: multiple states and proton transfer, *Proceedings of the National Academy of Sciences of the United States of America* 93, 8362-8367.
62. Brejc, K., Sixma, T. K., Kitts, P. A., Kain, S. R., Tsien, R. Y., Ormo, M., and Remington, S. J. (1997) Structural basis for dual excitation and photoisomerization of the *Aequorea victoria* green fluorescent protein, *Proceedings of the National Academy of Sciences of the United States of America* 94, 2306-2311.
63. Valeur, B., Berberan-Santos, M. N. (2012) *Molecular Fluorescence : Principles and*

Applications, Wiley-VHC Verlag GmbH, Weinheim.

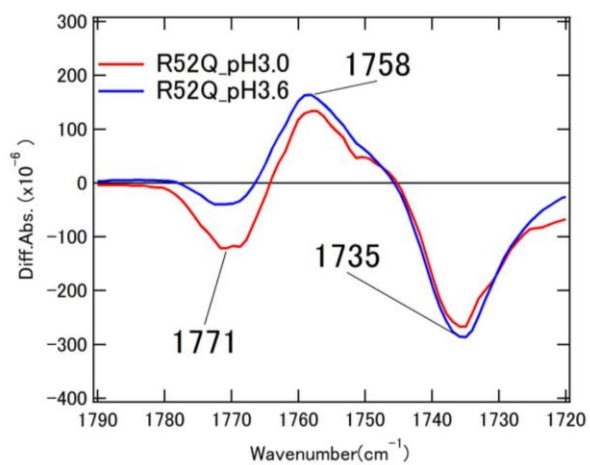
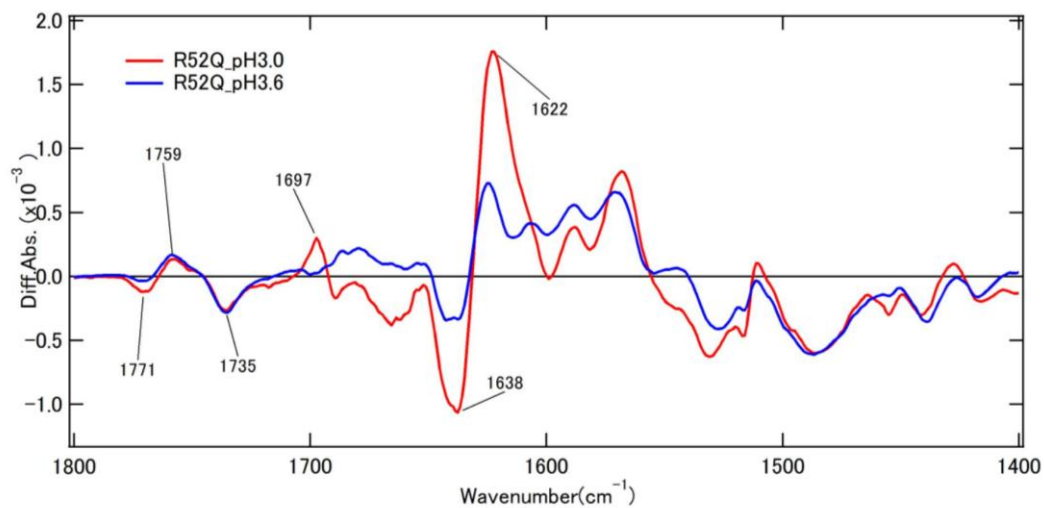
64. Lakowicz, J. R. (2006) *Principles of Fluorescence Spectroscopy*, 3rd edition ed., Springer Science + Business Media, New York.
65. Douhal, A., Lahmani, F., Zewail, A.H. (1996) Proton-transfer reaction dynamics, *Chemical Physics* 207(2-3), 477-498.
66. Harigai, M., Yasuda, S., Imamoto, Y., Yoshihara, K., Tokunaga, F., Kataoka, M. (2001) Amino acids in the N-terminal region regulate the photocycle of photoactive yellow protein, *Journal of Biochemistry* 130, 51-56.
67. Henry, N. P., Senozan, N. M. (2001) The Henderson-Hasselbalch equation : its history and limitations, *Journal of Chemical Education* 78, 1499-1503.
68. Tkachenko, N. V. (2006) *Optical Spectroscopy : Methods and Instrumentations*, Elsevier Science and Technology, Amsterdam.
69. Demchenko, A. P., editor (2010) *Advanced Fluorescence Reporters in Chemistry and Biology I : Fundamentals and Molecular Design*, Vol. 8, Springer-Verlag, Berlin Heidelberg.
70. Shynkar, V. V., Klymchenko, A.S., Piemont, E., Demchenko, A.P., Mely, Y. (2004) Dynamics of intermolecular hydrogen bonds in the excited states of 4'-dialkylamino-3-hydroxyflavones, on the pathway to an ideal fluorescent hydrogen bonding sensor, *Journal of Physical Chemistry A*. 108, 8151-8159.

71. Groenhof, G., Schafer, L. V., Boggio-Pasqua, M., Grubmuller, H., Robb, M. A. (2008) Arginine52 controls the photoisomerization process in photoactive yellow protein, *Journal of American Chemical Society* 130, 3250-3251.
72. Noji, M. (2013) Protonation state of R52 in PYPM intermediate, In *Graduate School of Materials Science Master Thesis*, Nara Institute of Science and Technology.
73. Boggio-Pasqua, M., Groenhof, G. (2011) Controlling the photoreactivity of the photoactive yellow protein chromophore by substituting at the p-coumaric acid group, *The Journal of Physical Chemistry B* 115, 7021-7028.
74. Virshup, A. M., Punwong, C., Pogorelov, T. V., Lindquist, B. A., Ko, C., Martinez, T. J. (2009) Photodynamics in complex environments: ab initio multiple spawning quantum mechanical/molecular mechanical dynamics, *The Journal of Physical Chemistry B* 113, 3280-3291.
75. Toniolo, A., Olsen, S., Manohar, L., Martinez, T. J. (2004) Conical intersection dynamics in solution: the chromophore of Green Fluorescent Protein, *Faraday Discuss* 127, 149-163.

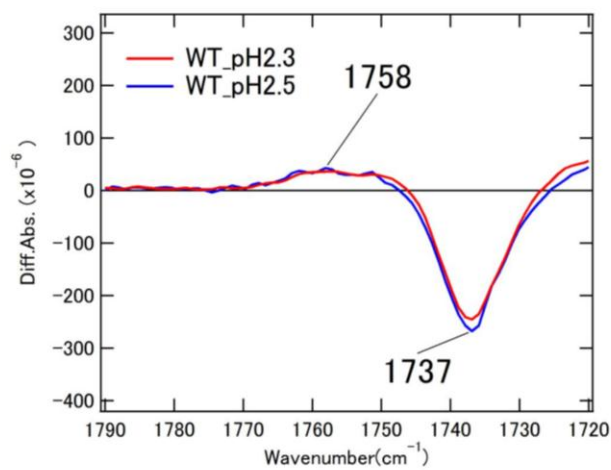
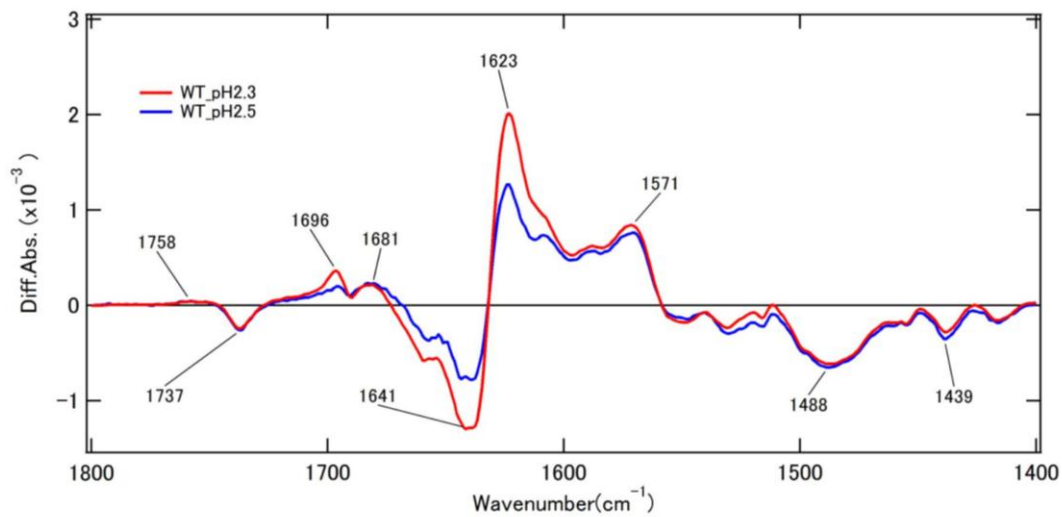
Appendix 1 : Far-UV Circular Dichroism Spectra of wtPYP-coumarin, R52Q-coumarin, and E46Q-coumarin.



Appendix 2. FTIR Difference Spectra of before and after reaction of light adapted state of R52Q.



Appendix 3. FTIR Difference Spectra of before and after reaction of light adapted state of wildtype PYP.



Appendix 4. Reconstructed spectral components data obtained by analyzing the decay with double exponential functions using global analysis.

Equation for double exponential function :

$$y = y_0 + Ae^{-\frac{(t-t_0)}{\tau_0}} + Be^{-\frac{(t-t_0)}{\tau_1}}$$

y_0 : y-axis offset

A, B : amplitude

τ_i : time constant

WtPYP-coumarin pH 2.1, excitation wavelength 365 nm, in 20 mM Tris HCl, RT

A (1 ns time window)	B (1 ns time window)	A (20 ns time window)	B (20 ns time window)	Wavelength (nm)
42.9407	1.78169	62.0885	14.1717	415.165
56.3885	3.8104	85.6089	21.2728	422.553
65.8293	5.20746	97.4892	25.3471	429.942
65.8828	9.08173	105.015	34.5705	437.331
63.2236	10.9849	104.709	41.5136	444.72
51.3194	17.2742	88.3014	56.3615	452.108
45.0902	22.211	79.379	78.9001	459.497
27.371	30.0887	62.185	91.8962	466.886
20.0556	27.913	37.4844	87.8971	474.275
15.2142	23.679	22.8158	71.9353	481.663
11.056	18.1685	21.4729	56.2387	489.052
8.9304	13.8097	10.3984	47.9653	496.441

WtPYP-coumarin pH 3.0, excitation wavelength 365 nm, in 20 mM Tris HCl, RT

A (1 ns time window)	B (1 ns time window)	A (20 ns time window)	B (20 ns time window)	Wavelength (nm)
6.2691	0.91808	11.3224	4.12683	415.165
9.05009	1.92498	17.4373	6.95208	422.553
10.0672	3.7135	28.6421	8.13585	429.942
14.985	3.95817	34.5528	12.04	437.331
15.7186	4.63462	31.9679	14.7581	444.72
16.1656	5.16858	39.8697	16.7721	452.108
13.3533	7.70042	26.7648	24.8475	459.497
11.2437	8.87751	20.8853	28.1538	466.886
9.01172	8.96622	16.4222	28.4383	474.275
8.09573	6.88049	7.9111	25.8083	481.663
5.09597	5.95435	14.1133	17.9105	489.052
3.71756	4.51885	9.50378	14.2043	496.441

R52Q-coumarin pH 3.0, excitation wavelength 365 nm, in 20 mM Tris HCl, RT

A (1 ns time window)	B (1 ns time window)	A (20 ns time window)	B (20 ns time window)	Wavelength (nm)
6.84948	0.314469	29.4662	4.09	415.165
11.9651	0.509887	38.8451	9.33336	422.553
18.5435	0.659179	56.5246	10.7865	429.942
21.6477	1.74843	70.2558	12.9655	437.331
24.7343	2.32995	70.1998	17.5639	444.72
25.8033	3.86626	75.1445	21.1248	452.108
25.6921	5.4497	67.0201	31.7302	459.497
21.2487	7.97697	56.9746	41.9096	466.886
17.0846	9.52512	41.893	38.3364	474.275
13.0048	7.81061	31.4529	33.8508	481.663
12.7307	5.44214	25.5175	27.5222	489.052
7.32568	5.5798	12.7885	22.6609	496.441

E46Q-coumarin pH 3.0, excitation wavelength 365 nm, in 20 mM Tris HCl, RT

A (1 ns time window)	B (1 ns time window)	A (20 ns time window)	B (20 ns time window)	Wavelength (nm)
17.1863	4.77576	18.5835	9.4702	415.165
29.7036	9.80374	29.9676	19.9331	422.553
44.8399	14.7393	61.0739	31.0872	429.942
58.6987	18.5318	84.923	37.1618	437.331
60.6562	22.4575	114.837	46.056	444.72
60.9219	25.3661	90.1277	63.6118	452.108
56.9105	27.9912	92.4758	79.817	459.497
21.73	16.7265	33.9218	53.0332	466.886
16.1075	16.8563	22.0394	52.7897	474.275
10.8975	14.4281	15.7601	45.6965	481.663
9.83576	10.6388	12.8748	34.8066	489.052
7.11635	8.28648	11.104	28.0322	496.441

WtPYP-coumarin pH 8.0, excitation wavelength 444 nm, in 20 mM Tris HCl, RT

A (1 ns time window)	B (1 ns time window)	A (20 ns time window)	B (20 ns time window)	Wavelength (nm)
27.0983	1.41613	6.4224	3.65515	452.108
90.4103	3.96364	11.5294	12.4887	459.497
138.643	7.51783	34.4403	23.4504	466.886
146.675	9.3341	40.8819	28.5176	474.275
143.204	8.7137	55.5307	26.3599	481.663
136.401	6.98457	64.0225	22.743	489.052
117.789	6.20113	52.1928	19.9747	496.44

R52Q-coumarin pH 8.0, excitation wavelength 444 nm, in 20 mM Tris HCl, RT

A (1 ns time window)	B (1 ns time window)	A (20 ns time window)	B (20 ns time window)	Wavelength (nm)
32.0329	5.62914	1.47931	6.17842	452.108
93.3657	18.3415	12.1787	19.1844	459.497
145.851	34.5732	11.3331	37.7432	466.886
158.989	41.1932	23.7731	50.7346	474.275
158.398	39.2016	27.7818	53.0315	481.663
145.837	34.0139	31.7532	55.304	489.052
119.846	29.2019	37.1002	53.8155	496.44

E46Q-coumarin pH 8.0, excitation wavelength 444 nm, in 20 mM Tris HCl, RT

A (1 ns time window)	B (1 ns time window)	A (20 ns time window)	B (20 ns time window)	Wavelength (nm)
5.55038	0.336496	0.383761	1.19353	452.108
21.1614	1.0267	0.488722	2.30969	459.497
50.4697	1.6625	2.41642	4.10669	466.886
66.7126	2.21112	0.06815	5.27092	474.275
65.9277	1.80526	3.85479	4.8236	481.663
62.5537	1.78648	2.35851	4.01092	489.052
62.6711	1.33307	11.9928	3.60882	496.44